Molecular Cell

Article

Lysosomal damage sensing and lysophagy initiation by SPG20-ITCH

Graphical abstract

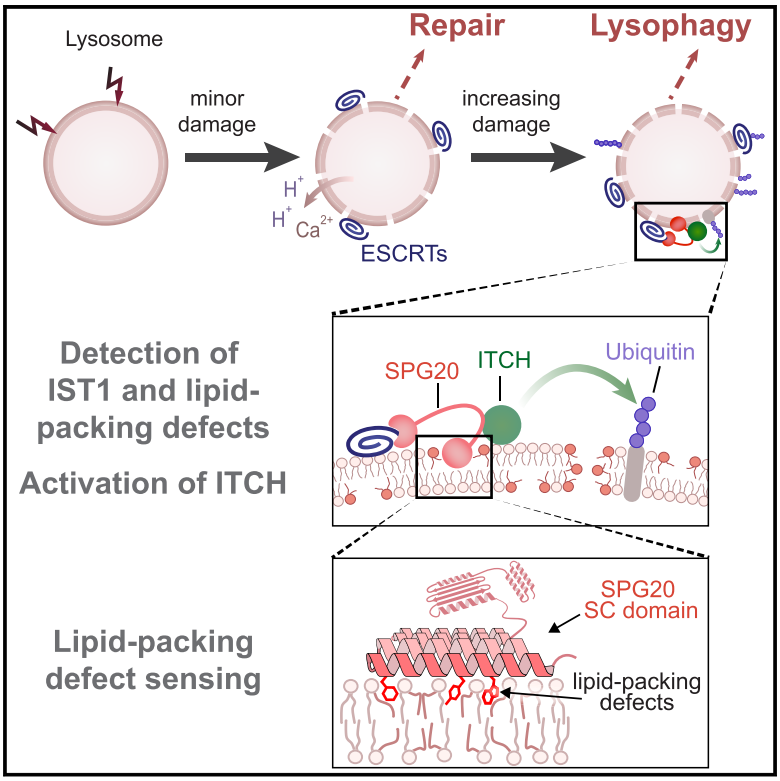

Authors

Pinki Gahlot, Bojana Kravic, Giulia Rota, ..., Simona Polo, Christian Behrends, Hemmo Meyer

Correspondence

hemmo.meyer@uni-due.de

In brief

How the decision is made between repair or lysophagy of damaged lysosomes in various conditions is largely unclear. Gahlot et al. identified a pathway consisting of the membrane sensor SPG20 and the ubiquitin ligase ITCH, which triages damaged lysosomes for lysophagy based on the extent of damage-associated lipid-packing defects.

Highlights

- Various types of lysosomal membrane damage are associated with lipid-packing defects
- SPG20 detects damage-associated lipid-packing defects in the limiting membrane
- SPG20 recruits and activates the ubiquitin ligase ITCH
- ITCH-mediated lysine-63-linked ubiquitylation triages lysosomes for lysophagy

Gahlot et al., 2024, Molecular Cell *84*, 1556–1569
April 18, 2024
https://doi.org/10.1016/j.molcel.2024.02.029

CellPress

CellPress
OPEN ACCESS

Molecular Cell

Article

Lysosomal damage sensing and lysophagy initiation by SPG20-ITCH

Pinki Gahlot,[1] Bojana Kravic,[1] Giulia Rota,[1] Johannes van den Boom,[1] Sophie Levantovsky,[2] Nina Schulze,[3] Elena Maspero,[4] Simona Polo,[4] Christian Behrends,[2] and Hemmo Meyer[1,5,*]
[1]Center of Medical Biotechnology, Faculty of Biology, University of Duisburg-Essen, Essen, Germany
[2]Munich Cluster for Systems Neurology, Medical Faculty, Ludwig-Maximilians-University München, Munich, Germany
[3]Imaging Center Campus Essen, Center of Medical Biotechnology, Faculty of Biology, University of Duisburg-Essen, Essen, Germany
[4]IFOM ETS, The AIRC Institute of Molecular Oncology, Milan, Italy
[5]Lead contact
*Correspondence: hemmo.meyer@uni-due.de
https://doi.org/10.1016/j.molcel.2024.02.029

SUMMARY

Cells respond to lysosomal membrane permeabilization by membrane repair or selective macroautophagy of damaged lysosomes, termed lysophagy, but it is not fully understood how this decision is made. Here, we uncover a pathway in human cells that detects lipid bilayer perturbations in the limiting membrane of compromised lysosomes, which fail to be repaired, and then initiates ubiquitin-triggered lysophagy. We find that SPG20 binds the repair factor IST1 on damaged lysosomes and, importantly, integrates that with the detection of damage-associated lipid-packing defects of the lysosomal membrane. Detection occurs via sensory amphipathic helices in SPG20 before rupture of the membrane. If lipid-packing defects are extensive, such as during lipid peroxidation, SPG20 recruits and activates ITCH, which marks the damaged lysosome with lysine-63-linked ubiquitin chains to initiate lysophagy and thus triages the lysosome for destruction. With SPG20 being linked to neurodegeneration, these findings highlight the relevance of a coordinated lysosomal damage response for cellular homeostasis.

INTRODUCTION

Lysosomes are the main degradative organelles in the cell and serve as key signaling platforms.[1] Loss of lysosomal function due to lysosomal membrane permeabilization (LMP) is therefore highly deleterious and can induce inflammation and even cell death.[2,3] Various conditions cause LMP, including lipid bilayer perturbation in the limiting membrane of the lysosome due to changes in lipid composition, lipid peroxidation, or membranolytic agents.[2,3] In addition, crystals, neurotoxic aggregates, or bacteria can puncture or fully rupture endolysosomal membranes.[2,3] Notably, LMP is relevant for human health because it is associated with neurodegeneration and infection[4–7] and can represent a significant vulnerability in cancer cells.[8,9]

Cells respond to LMP by rapid recruitment of endosomal sorting complexes required for transport (ESCRT).[10,11] Generally, the ESCRT machinery comprises complexes ESCRT-0, -I, -II, and -III. ESCRT-III components (including CHMPs 1–7 and IST1) form concentric filaments on the membrane surface, which are thought to constrict sites of permeability to seal the membrane.[12,13] In addition, LMP can be mitigated by lipid scrambling and phosphoinositide-regulated transport of lipids from the ER at ER-lysosome contact sites.[14–16] Alternatively, likely if damage is too extensive to be repaired, damaged lysosomes can be triaged as a whole for degradation by lysophagy. Lysophagy is initiated by ubiquitylation of lysosomal proteins.[17–19] In line with that, pharmacological inhibition of ubiquitylation blocks lysophagy.[20] An initial pulse of lysine-63-linked (K63) ubiquitylation recruits autophagy receptors such as p62/SQSTM1, OPTN (optineurin), and TAX1BP1, followed by extensive formation of K48 chains during later stages of the damage response.[20–23] The ubiquitin chains and autophagy receptors induce and recruit the LC3-decorated phagophore for engulfment of the damaged lysosome and subsequent fusion with intact lysosomes for degradation.[18,19,21]

How the decision is made between repair and lysophagy of damaged lysosomes and how unrepairable damage is sensed so as to initiate K63 ubiquitylation that triggers lysophagy is not fully understood. If damage is extensive with large pore formation, the resulting exposure of luminal glycans acts as a damage signal. Glycans are sensed either directly by ubiquitin ligase components such as FBXO2 and FBXO27 that trigger ubiquitylation of lysosome components in some cell types or by cytosolic galectins that initiate downstream events leading to lysophagy.[6,7,24,25] However, lysophagy may be required and beneficial before the limiting membrane disintegrates, particularly in sterile stress and disease conditions associated with lipid perturbations. We hypothesized that the Troyer syndrome protein SPG20 (also called spartin) may be a critical regulator in these conditions. SPG20 can bind membranes, and proteomics indicated that SPG20 associates with

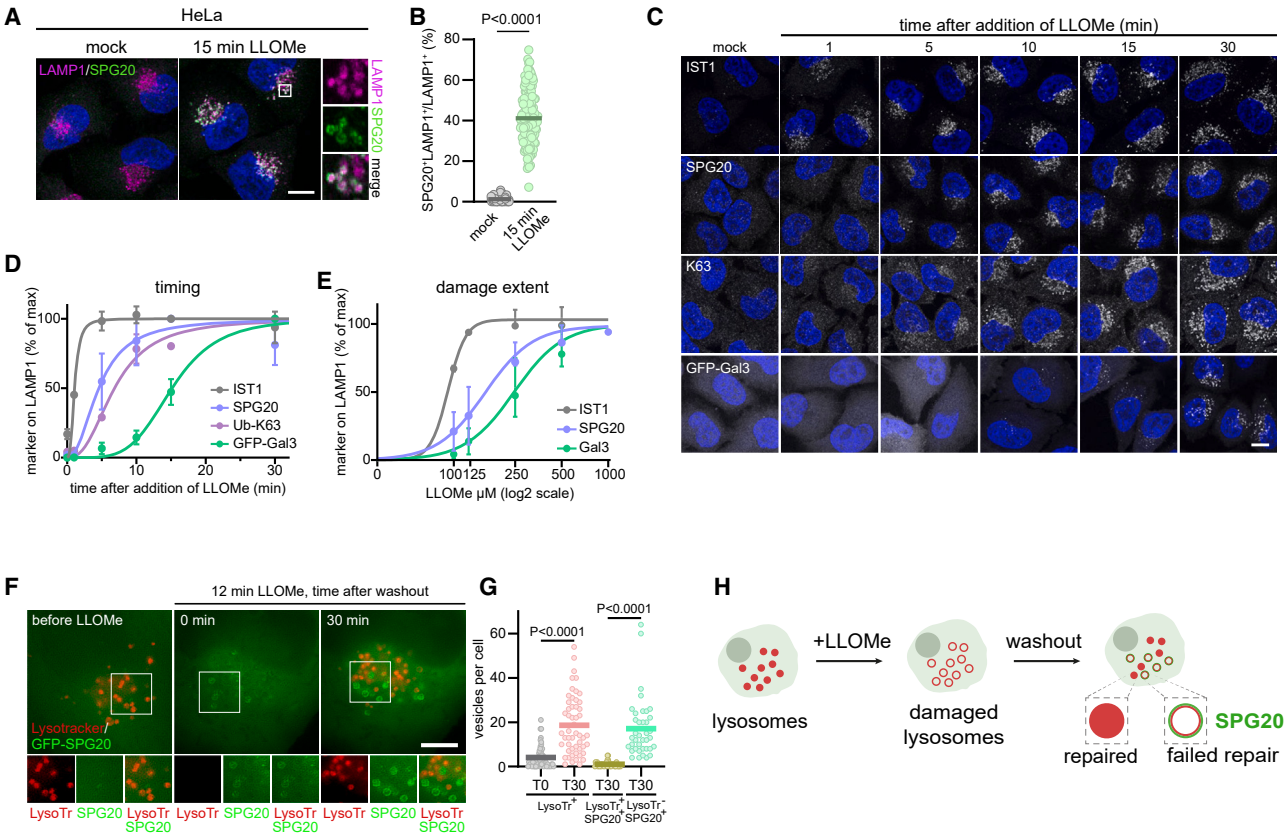

Figure 1. SPG20 marks damage-induced initiation of lysophagy

(A) Translocation of endogenous SPG20 to damaged lysosomes. HeLa cells were mock or LLOMe-treated (1 mM) and costained for SPG20 and LAMP1.

(B) Quantification of (A).

(C) HeLa cells were fixed at different time points after LLOMe addition (1 mM) and stained for indicated markers. Note coinciding SPG20 recruitment and K63 ubiquitylation after IST1 and before Gal3 translocation.

(D) Quantification of (C).

(E) Recruitment of indicated factors with increasing damage extent. Cells were treated for 15 min with indicated increasing LLOMe concentrations, and recruitment of markers was quantified. See Figure S2C for corresponding microscopy images.

(F) Live-cell 2D-SIM analysis of lysosome repair. HeLa cells expressing GFP-SPG20 and loaded with pH-sensitive LysoTracker were imaged before and after a 12 min LLOMe pulse (1 mM), and 30 min after washout. Note that SPG20 localized to lysosomes that failed to recover. See Figure S2D for OPTN localization.

(G) Quantification of (F).

(H) Triaging of lysosomes into repaired and unrepaired lysosomes.

Statistics: (B, D, and E) n = 3 biologically independent experiments, with >20 cells quantified per condition. (F and G) >30 cells quantified for each time point. (B and G) Lines indicate median. (D and E) Error bars, SD. (B) Unpaired t test. (G) One-way ANOVA with Tukey's multiple comparison test. (D and E) Allosteric sigmoidal fit. Scale bars: 10 µm in (A) and (C) and 5 µm in (F).

damaged lysosomes.[26] Moreover, SPG20 activates members of the Nedd4-like HECT-domain ubiquitin ligases known to regulate membrane trafficking through K63 ubiquitylation.[27,28] Here, we show that SPG20 senses lipid-packing defects in the limiting membrane associated with lysosomal damage. If lipid perturbations are extensive, SPG20 recruits and activates the ubiquitin ligase ITCH to trigger K63-linked ubiquitylation and so initiates lysophagy.

RESULTS

SPG20 marks damage-induced initiation of lysophagy

We first confirmed recruitment of SPG20 to damaged lysosomes in HeLa and U2OS cells, as well as in ARPE-19 retinal pigment epithelia and SH-SY5Y neuroblastoma cells, by immunofluorescence microscopy (Figures 1A, 1B, and S1A–S1D). Lysosomal damage was induced by treatment of cells with L-leucyl-L-leucine methyl ester (LLOMe). LLOMe is membrane-permeable and lysosomotropic and is rapidly converted by cathepsin C to membranolytic poly-leucine peptides that accumulate in lysosomes and permeabilize the limiting membrane.[29]

To explore whether SPG20 recruitment may have relevance in lysophagy initiation, we first assessed the timing of SPG20 recruitment to damaged lysosomes and its relation to K63 ubiquitylation and compared it with translocation of the ESCRT component IST1 and the damage marker galectin-3 (Gal3). Gal3 is a lectin present in the cytosol that enters damaged

lysosomes through larger perforations or ruptures and is then trapped on luminal β-galactosides.[7,21] Markers were imaged by immunofluorescence microscopy followed by automated quantification in cells fixed at different time points after LLOMe addition (Figures 1C and 1D). As expected, IST1 was fully recruited within 5 min with a half-maximal recruitment already at 1 min after addition of LLOMe at relatively high concentrations (1 mM). Of note, SPG20 translocated shortly after IST1 with half-maximal signal at 5 min. Importantly, SPG20 translocation coincided with the emerging K63 ubiquitin chains suggesting that K63 ubiquitylation was linked to SPG20 recruitment. By contrast, Gal3 was recruited significantly later with a maximum level reaching at 30 min, as previously reported.[10] Costaining revealed that SPG20, and later SPG20 and Gal3, localized to CHMP4B-positive lysosomes indicating that different damage responses can occur successively on a single lysosome when damage is increasing (Figures S1E and S1F).

We next treated HeLa cells with a range of LLOMe concentrations (100 μM to 1 mM). We observed increasing proton leakage rates as detected by loss of lysotracker fluorescence that correlated with rising LLOMe concentrations confirming that treatments induced a gradual degree of damage (Figures S2A and S2B). In treated cells, IST1 responded with maximal translocation already at low LLOMe concentrations (Figures 1E and S2C) consistent with ESCRT recruitment being triggered by Ca^{2+} and with Ca^{2+} release from lysosomes being pH-sensitive.[10,30] By contrast, SPG20 translocation occurred at a higher threshold of damage suggesting it required a different additional trigger than IST1 (Figures 1E and S2C). Again, SPG20 translocation was uncoupled from Gal3, which required even higher LLOMe concentrations, indicating that SPG20 responds already to damage levels that are less severe than those required for Gal3 translocation.

Upon damage, a fraction of lysosomes is expected to be repaired, whereas other lysosomes are damaged too severely and triaged for lysophagy. We therefore next asked to which fraction of lysosomes SPG20 was recruited. We performed live-cell 2D-SIM microscopy of cells loaded with lysotracker and expressing GFP-SPG20 (Figures 1F and 1G). We applied a short pulse with a high LLOMe concentration (1 mM) followed by washout to ensure acute damage. A 12 min LLOMe pulse sufficed to lead to proton loss in the majority of lysosomes as detected by lysotracker. Of note, SPG20 partially translocated to lysotracker-negative structures already during the pulse. Many lysosomes recovered within the 30 min chase after LLOMe washout demonstrating that repair was successful in these lysosomes. Notably, SPG20 preferentially translocated to those lysosomes that failed to recover (Figures 1F and 1G). Moreover, the autophagy receptor OPTN followed SPG20 on these lysosomes (Figures S2D and S2E), showing that lysophagy was initiated. Thus, during the lysosomal damage response, SPG20 marks the triaging event leading to lysophagy (Figure 1H).

SPG20 recruits and activates ITCH on damaged lysosomes

SPG20 binds and activates members of the Nedd4-like family of ubiquitin ligases directly by interaction of the PPAY motif with WW domains of the ligase[27] (Figure 2A). To identify the specific ligase that is activated during the response to lysosomal damage, we screened the Nedd4-like family by overexpressing GFP or YFP-tagged versions. Only YFP-ITCH translocated to lysosomes after LLOMe treatment (Figure S3A). We confirmed recruitment of endogenous ITCH to damaged lysosomes where it colocalized with SPG20 (Figures 2B and 2C). KO or depletion of SPG20 largely reduced ITCH localization on damaged lysosomes indicating that ITCH recruitment was mediated by SPG20 (Figures 2D, 2E, and S3B–S3E). Moreover, co-immunoprecipitation showed that SPG20 translocation to damaged lysosomes correlated with an LLOMe-induced increase in binding of SPG20 and ITCH by the PPAY motif in SPG20 (Figure 2F). Importantly, ITCH was activated by LLOMe-induced damage as evidenced by ubiquitylation of ITCH that was auto-catalyzed because it was abolished in the case of the inactive ITCH C871A variant (Figure 2G). Moreover, ITCH autoubiquitylation was reduced in SPG20 KO cells showing that damage-induced activation of ITCH was facilitated by SPG20 (Figure 2H).

Of note, activated ITCH was critical for early steps of lysophagy, because KO or depletion of ITCH in HeLa cells reduced K63 ubiquitylation of damaged lysosomes, and also affected K48 ubiquitylation to a lesser degree (Figures 2I, 2J, and S3F–S3K). K63 ubiquitylation in ITCH KO cells was rescued by overexpression of wild-type ITCH but not of the catalytically inactive ITCH C871A mutant (Figures 2I and 2J). In line with the role of SPG20 in recruiting ITCH, also SPG20 depletion in HeLa cells largely reduced K63 ubiquitylation of damaged lysosomes, as expected (Figures S3L and S3M). We confirmed that SPG20 was required for K63 ubiquitylation also in ARPE19 and SH-SY5Y cells (Figures S3N–S3S). To further explore damage-induced ubiquitylation by ITCH, we performed ubiquitin remnant profiling of LLOMe-treated cells and compared ITCH knockout cells with parental HeLa cells. We detected ubiquitylation of lysosomal and trafficking factors in LLOMe-treated parental cells and its reduction in ITCH KO cells (Figures S4A–S4E; Tables S1 and S2). With the limitation that we did not include unchallenged cells in the comparison, the analysis suggests that these factors are targets of ITCH during the damage response. Among the potential targets, we identified lysosomal repair machinery including the ESCRT components PDCD6IP/ALIX, HGS, STAM, and IST1. We confirmed ITCH-dependent IST1 ubiquitylation in LLOMe-treated, but not in unchallenged cells, by denaturing pull-down and western blot (Figure S4F), supporting the notion that ITCH acts on lysosomes undergoing default repair attempts.

SPG20 and ITCH regulate lysophagy initiation

Further functional analysis demonstrated that SPG20 and ITCH were crucial for key steps in lysophagy. First, ITCH or SPG20 KO resulted in compromised clearance of Gal3-decorated damaged lysosomes over time (Figures S5A–S5D) indicating a prime role in the lysosomal damage response. The clearance defect in the KO cells could be rescued by ectopic expression of the respective wild-type proteins (Figures S5A–S5D). Notably, the defect was not rescued by the SPG20 PPAY motif mutant, which cannot activate ITCH, or by the inactive ITCH C871A mutant (Figures S5A–S5D), demonstrating that ITCH activation by SPG20 and ITCH-mediated ubiquitylation is

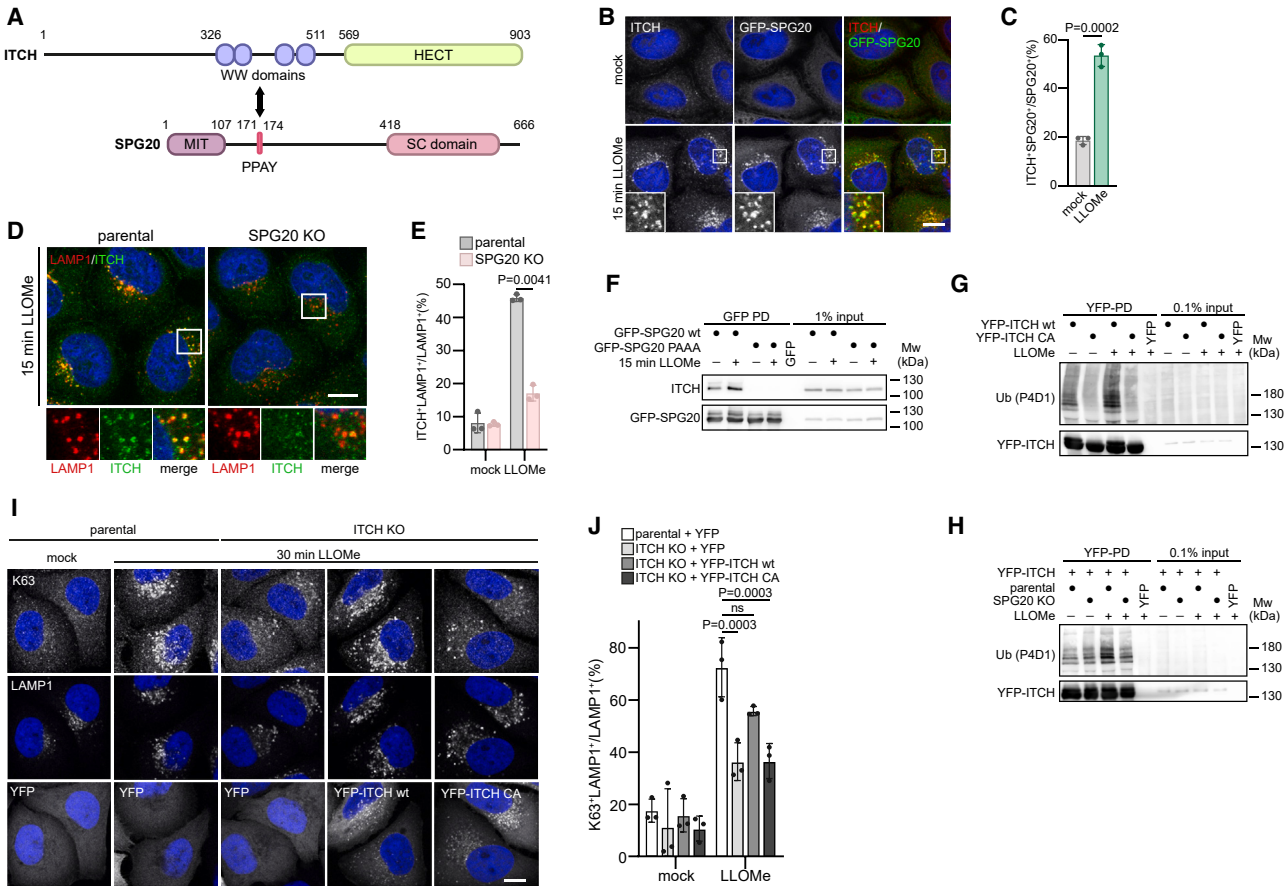

Figure 2. SPG20 recruits and activates ITCH on damaged lysosomes

(A) Domain structures of SPG20 and ITCH. HECT, catalytic ubiquitin ligase domain; SC domain, plant-related senescence domain; MIT, microtubule interacting and trafficking domain.

(B) ITCH is recruited to damaged lysosomes and colocalizes with SPG20. Cells expressing GFP-SPG20 were mock or LLOMe-treated as indicated and stained for ITCH.

(C) Quantification of (B).

(D) ITCH recruitment depends on SPG20. Control or SPG20 knockout cells were treated and stained for ITCH and LAMP1.

(E) Quantification of (D).

(F) Interaction between SPG20 and ITCH. GFP-SPG20 wild type (WT) or a mutant of the PPAY motif (PAAA) were mock or LLOMe-treated followed by lysis and GFP pull-down (PD). Note increased interaction upon LLOMe-treatment which was abolished by the PAAA mutation.

(G) Lysosomal damage induces activation of ITCH. Cells expressing YFP-ITCH WT or catalytically inactive ITCH C871A (CA) mutant were mock or LLOMe-treated, and lysates subjected to ITCH immunoprecipitation after denaturation. Western blot with ubiquitin antibody (P4D1).

(H and I) (H) ITCH autoubiquitylation, assessed as in (G), was compared between WT and SPG20 KO cells (I) ITCH mediates K63 ubiquitylation of damaged lysosomes. Parental HeLa or ITCH KO cells overexpressing YFP alone or YFP-tagged ITCH wild type or catalytically inactive CA mutant were fixed after mock or LLOMe treatment (250 μM) and costained for K63 ubiquitin chains and LAMP1 as indicated.

(J) Quantification of (H).

Statistics: all quantifications n = 3 biologically independent experiments, with >25 cells quantified per condition. (C, E, and J) Error bars, SD. (C) Unpaired t test. (E and J) Two-way ANOVA with Sidak's multiple comparison test. Scale bars: 10 μm in (B), (D), and (I).

critical for lysophagy of damaged lysosomes. Moreover, knockout of ITCH, like knockout of SPG20, impaired the recruitment of the autophagy receptors TAX1BP1 and p62 upon lysosomal damage in HeLa cells (Figures S6A–S6D). Consequently, the SPG20 or ITCH knockouts also reduced coalescence of LC3 around damaged lysosomes (Figures 3A and 3B), which we confirmed in ARPE19 cells depleted of SPG20 or ITCH (Figures S6E and S6F). Defective phagophore formation was mirrored by reduced LLOMe-induced LC3 lipidation in HeLa SPG20 knockout cells (Figures S6G and S6H). We next generated cell lines expressing pH-sensitive fluorescent protein mKeima fused to the lysosomal membrane protein TMEM192, equivalent to a recently characterized lysophagy reporter cell line.[31] The localization of the reporter at the cytosolic side of the membrane ensured that mKeima sensed acidification only due to lysophagy but not due to repair. Depletion of either SPG20 or ITCH largely reduced mKeima acidification compared with control (Figures 3C and 3D) confirming requirement of ITCH and SPG20 for lysophagy. In line with a central role of ITCH and SPG20 in the lysosomal damage

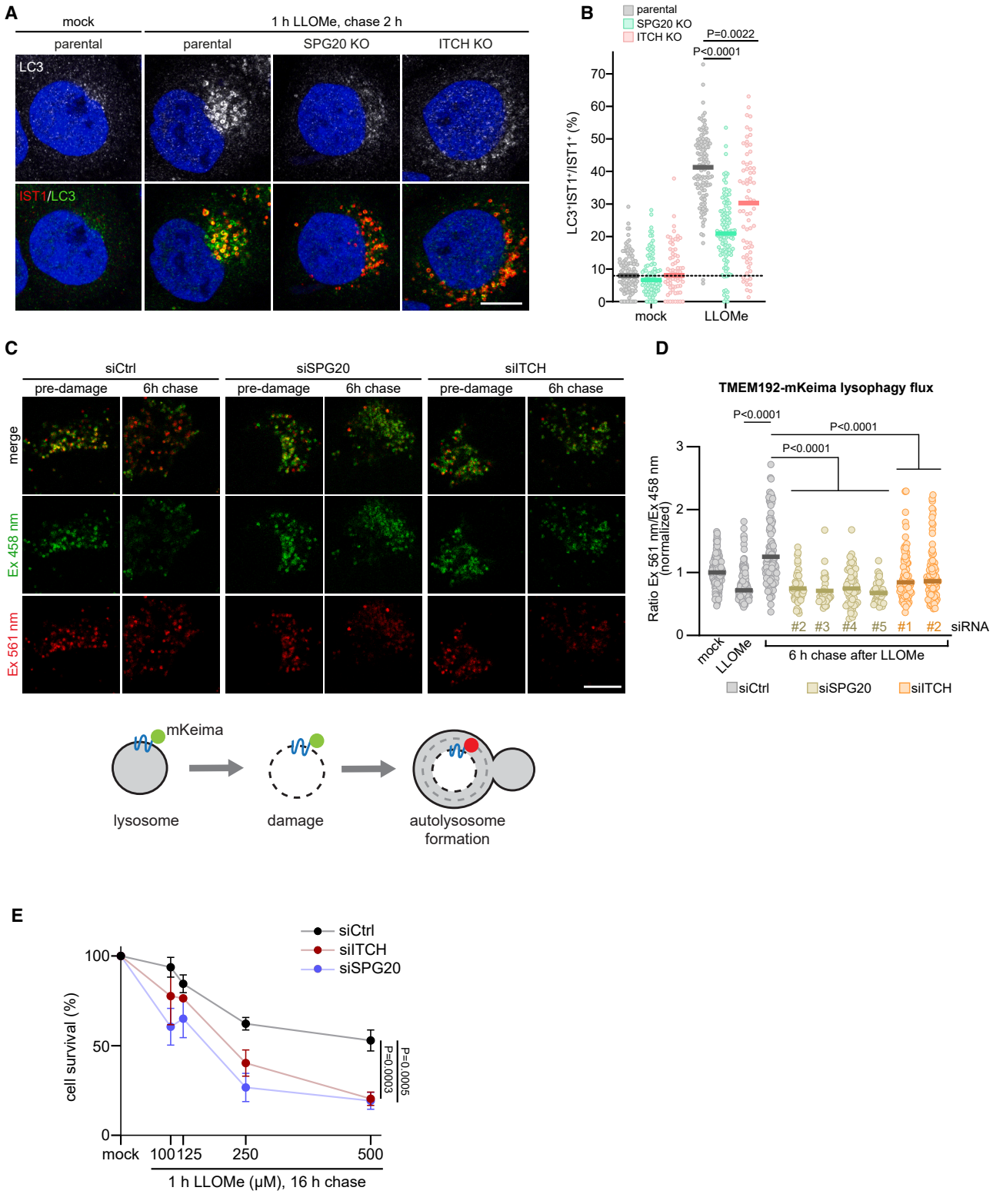

Figure 3. ITCH and SPG20 are required for efficient lysophagy

(A) Parental HeLa cells, or ITCH KO or SPG20 KO cells, were mock or LLOMe-treated (250 μM) for 1 h followed by 2 h chase and costained for IST1 and LC3.
(B) Quantification of (A).

(legend continued on next page)

response, depletion of either factor largely reduced cell survival upon LLOMe treatment (Figure 3E). Thus, the SPG20-ITCH pathway is important for initiation of lysophagy.

The SC domain recruits SPG20 to damaged lysosomes

We next asked how SPG20 detects damaged lysosomes to activate ITCH. SPG20 contains an MIT domain that specifically binds the ESCRT-III protein IST1[32] (Figure 4A). Co-immunoprecipitation demonstrated that IST1 bound SPG20 upon lysosomal damage and that this interaction was dependent on the MIT domain in SPG20 (Figure 4B). Deletion of the MIT domain in SPG20 or depletion of IST1 reduced the translocation of SPG20 to lysosomes, yet only partially (Figures 4C–4F), indicating that binding to IST1 helps direct SPG20 to damaged lysosomes but is not the prime determinant. Further SPG20 domain mapping showed that the C-terminal SC domain of SPG20 was essential and sufficient for binding to damaged lysosomes when overexpressed (Figures 4G and 4H). This is in line with previous reports that the SC domain can mediate membrane binding[33,34] (Figure 4A). We therefore asked whether membrane binding by the SC domain was triggered by damage-induced phosphatidylinositol-4-phosphate (PI4P), which was recently identified to be generated by PI4 kinase type 2α (PI4K2A) on damaged lysosomes and to govern repair by lipid transfer from the ER.[15,16] However, depletion of PI4K2A by small interfering RNA (siRNA) or knockout of PI4K2A had no effect on damage-induced SPG20 recruitment (Figures S7A and S7B) indicating that other features of the damaged membrane determine binding of SPG20.

SPG20 senses lipid-packing defects on damaged lysosomes

LLOMe condenses to short poly-leucine peptides that then partition into the lipid bilayer where they increase permeability by perturbing lipid packing.[35–37] Defects in lipid packing are best studied in highly curved membranes but can occur in flat membranes of organelles depending on the composition of the lipid bilayer.[38,39] We therefore asked whether LLOMe-induced perturbation in lysosomes coincided with generation of lipid-packing defects. We used an established amphipathic lipid-packing sensor (ALPS) consisting of a helical region of ARFGAP1 fused to mCherry.[38] Notably, the ALPS specifically translocated to LLOMe-damaged lysosomes and there colocalized with SPG20 (Figures 5A, 5B, S8A, and S8B). As expected, translocation of the ALPS to damaged lysosomes was reduced by mutations that interfere with packing-defect sensing (ALPS-SH) (Figures 5A, 5B, S8A, and S8B).

We next asked whether SPG20 may itself bind lipid-packing defects associated with lysosomal membrane damage and thereby sense the degree of lysosomal damage by the SC domain. AlphaFold predicted four amphipathic helices in the SC domain, arranged in a bundle with the hydrophobic regions pointing to one side (Figure 5C). Notably, the amphipathic helices 1 and 3 of the SC domain in SPG20 harbor bulky hydrophobic residues that are typical for ALPS (Figure 5C). Generally, in ALPS, these residues make contact with exposed acyl groups between phospholipid headgroups where lipids are loosely packed[38] and their substitution with the small hydrophobic residue valine specifically compromises sensing of lipid-packing defects while maintaining the amphipathicity.[40,41] We generated 3 mutant proteins in which we changed 6, 8, or 23 of the bulky hydrophobic residues to the small hydrophobic valine, termed 6xV, 8xV, and 23xV, respectively (Figures 5D–5F). Cellular expression of the proteins was not affected by the mutations (Figure S8C).

Of note, whereas the 6xV set of mutations already reduced translocation of SPG20 to damaged lysosomes in HeLa cells, translocation was largely abolished for the 8xV and 23xV mutants (Figures 5D and 5E), indicating that the SC domain of SPG20 has an ALPS motif to sense lipid-packing defects associated with lysosomal damage. The binding of damage-associated lipid-packing defects seen for SPG20 did not occur for any type of amphipathic helices because the ALPS of GMAP-210 or full-length PLIN3, which contains amphipathic helices, were not recruited, demonstrating a degree of specificity (Figures S8D and S8E). By contrast, ALPS-mediated recruitment of SPG20, but not of the 8xV mutant, was confirmed also in ARPE19 cells (Figures S8F and S8G). Importantly, unlike wild-type SPG20, the 8xV mutant was unable to restore ITCH recruitment in SPG20 KO cells (Figures 5G, 5H, and S8H). However, translocation of the SPG20 8xV mutant and ITCH recruitment to damaged lysosomes could be rescued by a fusion of the ALPS motif of ARFGAP1 to SPG20 8xV, demonstrating that sensing of lipid packing defects by SPG20 recruits SPG20 and ITCH to damaged lysosomes (Figures 5G, 5H, and S8H). Likewise, SPG20 wild-type and SPG20 8xV fused to the ARFGAP1-ALPS, but not the 8xV mutant alone, could rescue clearance of Gal3 vesicles after lysosomal damage (Figures S8I and S8J).

SPG20 detects lipid-packing defects induced by lipid peroxidation

To exclude that detection of lipid-packing defects was restricted to LLOMe-induced lipid bilayer perturbation, we resorted to lipid peroxidation.[23,42] Lipid peroxidation is associated with various conditions including neurodegeneration[2,3] and causes permeabilization and lipid-packing defects due to lipid truncation and the extra space taken by lipid hydroperoxides.[43,44] We induced lipid

(C and D) Lysophagy assay and quantification. HeLa cells stably expressing pH-sensitive mKeima fused to TMEM192. Due to its position on the cytosolic side of the lysosomal membrane, mKeima is acidified and shifts its excitation maximum from green to red during lysophagy but not during lysosome repair. Cells transfected with indicated siRNAs and treated with LLOMe followed by washout. mKeima fluorescence was assessed at both excitation wavelengths, and the ratio between both intensities was determined. Note that the ratio of red to green-excitable mKeima increases during 6 h chase indicating lysophagy, but this is largely reduced in SPG20 and ITCH-depleted cells.

(E) Cell survival during a 16 h chase after LLOMe-induced lysosomal damage of cells depleted with indicated siRNAs.

Statistics: (B) n = 3 biologically independent experiments with >25 cells quantified per condition. (D) n = 3 (for siSPG20 #3, #4, and #5 n = 1) biologically independent experiments with >30 cells quantified per condition. (E) n = 3 biologically independent experiments. (B) Mixed-effects analysis with Sidak's multiple comparison test. (D) One-way ANOVA with Tukey's multiple comparison test. Line indicates median (B) or mean (D). (E) Two-way ANOVA with Dunnett's multiple comparison test. (E) Error bars SD. Scale bars: 10 μm in (A) and (C).

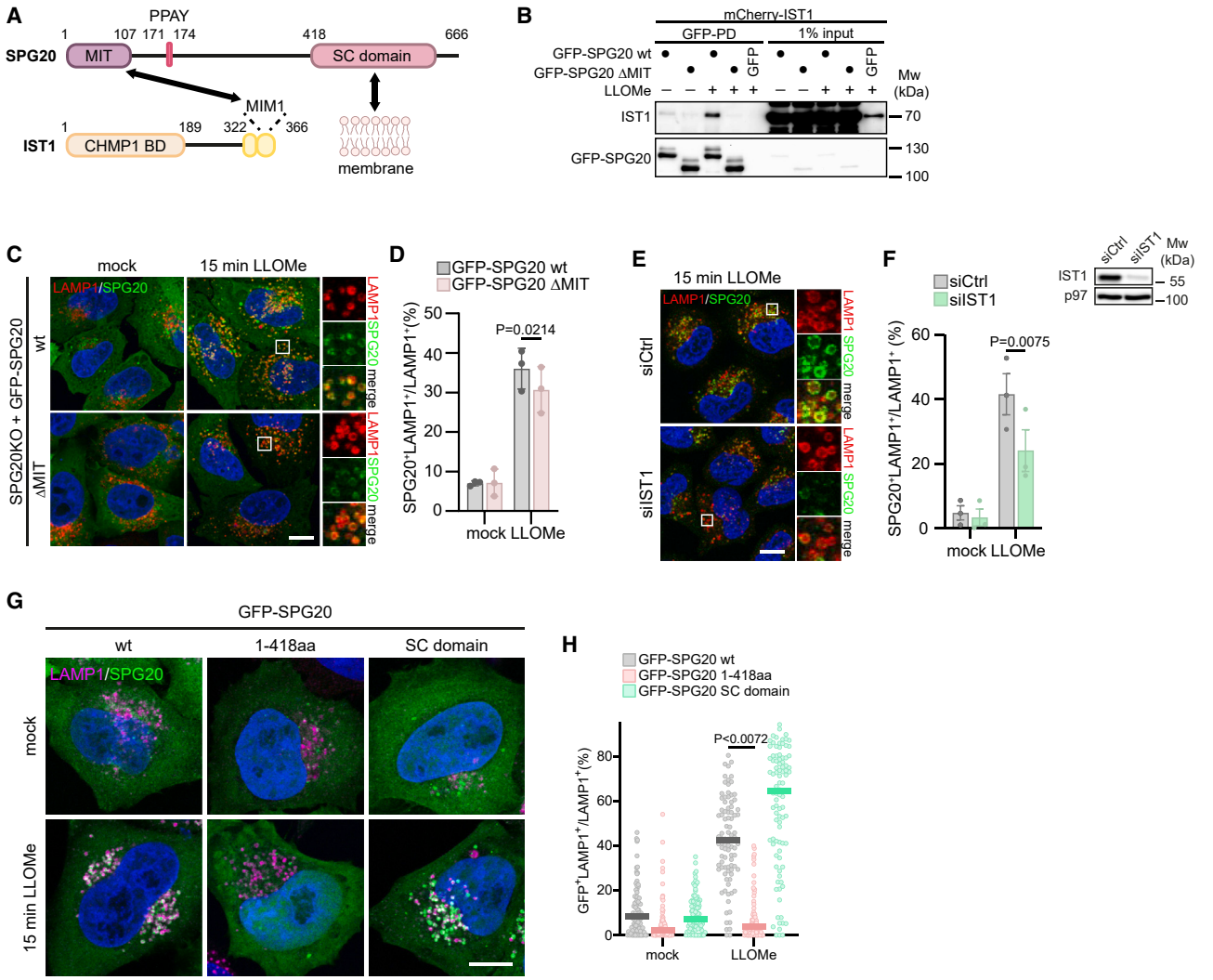

Figure 4. SPG20 translocation to damaged lysosomes primarily depends on the SC domain

(A) Domain structures of SPG20 and IST1. MIM1, MIT-interacting motif 1.

(B) LLOMe induces SPG20 binding to IST1 through the SPG20-MIT domain. Pull-down (PD) of GFP or GFP-SPG20 from cells after mock or LLOMe treatment.

(C) SPG20 translocation to damaged lysosomes only partially depends on the MIT domain. Cells expressing GFP-SPG20 wild-type or ΔMIT mutant stained for LAMP1 after mock or LLOMe treatment.

(D) Quantification of (C).

(E) SPG20 and LAMP1 costaining after LLOMe treatment in control or IST-depleted cells.

(F) Quantification of (E) and western blot confirmation of siRNA-mediated knockdown of IST1.

(G) Cells expressing GFP-SPG20 wild type, a truncation lacking the SC domain (1–418), or the SC domain alone stained for LAMP1 after mock or LLOMe (1 mM) treatment.

(H) Quantification of (G).

Statistics: all quantifications n = 3 biologically independent experiments with >30 cells quantified per condition. (D) Error bars, SD. (F) Error bars, SEM. (H) lines indicate median. (D, F, and H) Two-way ANOVA with Sidak's multiple comparison test. Scale bars: 10 μm in (C), (E), and (G).

peroxidation in three ways. First, we loaded lysosomes with the photosensitizer AlPcS2a that, when excited by light, generates radicals leading to peroxidation of unsaturated acyl chains in the membrane.[23] Notably, laser-irradiation of sensitizer-loaded lysosomes triggered rapid translocation of SPG20 (Figures 6A and S9A). Likewise, cellular uptake of nano-silica, which generates oxidizing radicals on their surface and causes lipid peroxidation,[45] or treatment with the palmitoyl-protein thioesterase 1 inhibitor DC661 that induces lipid peroxidation,[46] led to damage of lysosomes and recruitment of SPG20 (Figures S9B and S9C). Importantly, lysosomal translocation of SPG20 due to photosensitizer or silica-induced lipid peroxidation again depended on bulky hydrophobic residues as it was abolished by the 8xV and 23xV mutations (Figures 6A, S9A, and S9B) indicating that SPG20 senses lipid-packing defects on lysosomal membranes undergoing lipid peroxidation. By contrast, treatment with the TRPML1 agonist

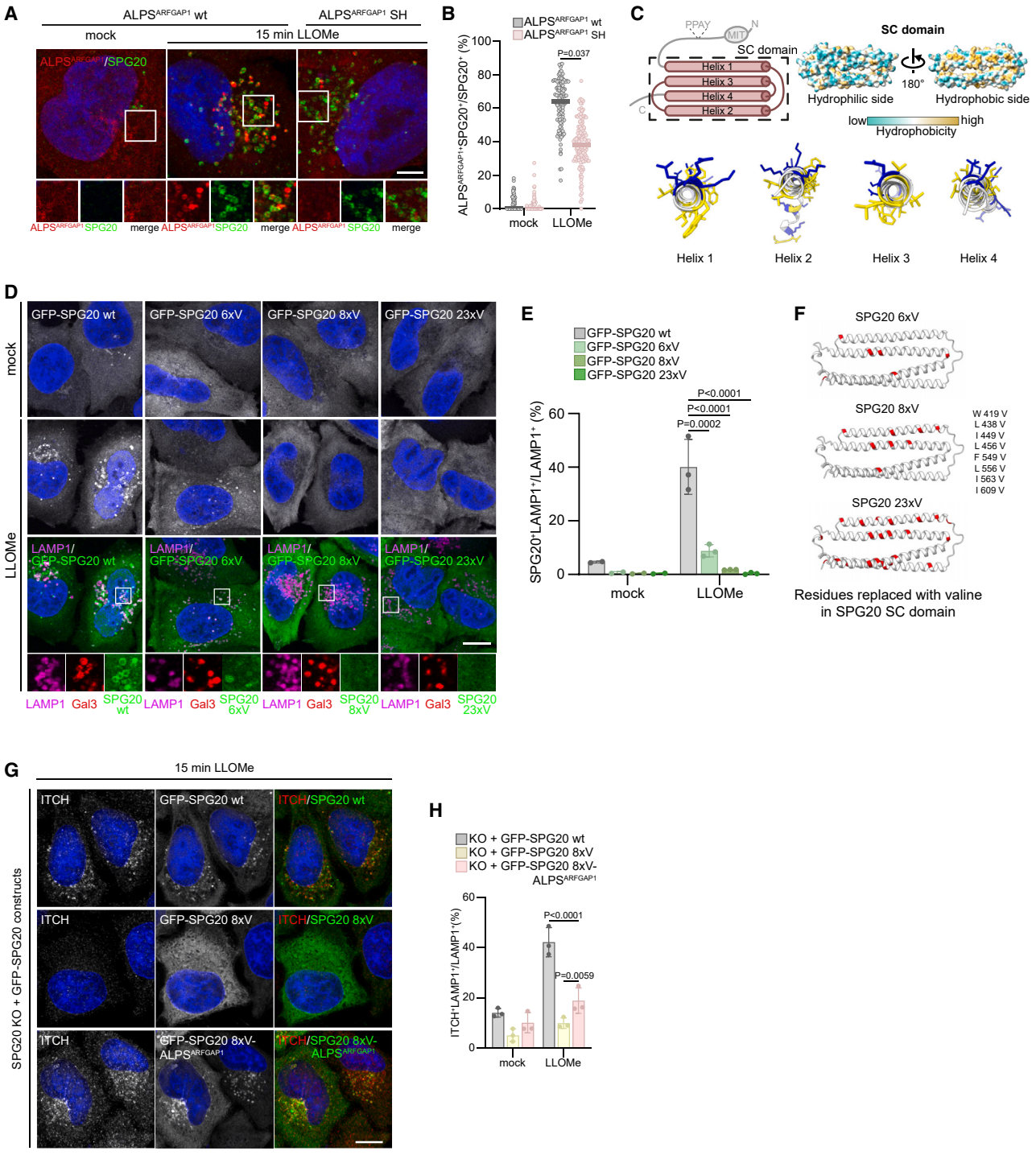

Figure 5. SPG20 senses lipid-packing defects on damaged lysosomes

(A) Lysosomal damage detected by SPG20 is associated with lipid-packing defects. Cells expressing mCherry fusions of the amphipathic lipid-packing sensor (ALPS) derived from ARFGAP1 or an ALPS mutant where bulky hydrophobic residues are substituted with small hydrophobic residues (SH mutant) were mock or LLOMe-treated and costained for SPG20 and LAMP1. See Figure S8A for LAMP1 staining.

(B) Quantification of colocalization of the ALPS^{ARFGAP1} with SPG20 in (A).

(C) Cartoon and AlphaFold prediction of the SC domain structure. Predicted cross-section through SC domain helices 1 and 3 with bulky hydrophobic residues (yellow) and charged residues (blue) highlighted.

(D) Translocation of SPG20 to damaged lysosomes depends on bulky hydrophobic residues in the SC domain. Cells expressing GFP-tagged versions of SPG20 wt, 6xV, 8xV, or 23xV mutant were mock or LLOMe-treated and costained for LAMP1 and Gal3.

(legend continued on next page)

ML-SA1, which releases Ca^{2+} from lysosomes without generating lipid-packing defects, induced recruitment of IST1, as expected, but did not lead to SPG20 translocation showing that SPG20 requires lipid perturbation and that IST1 alone is not sufficient to recruit SPG20 (Figure S9D).

To confirm this directly in a cell-free system, we performed membrane binding of SPG20 with giant unilamelar vesicles (GUVs). For induction of peroxidation, we incorporated the AlPcS2a photosensitizer. Gradual laser irradiation led to typical deformations of the GUVs that indicate peroxidation-induced perturbation of lipid packing and increase of surface area[43,47] (Figure 6B). We incubated the GUVs with purified SPG20 generated in insect cells and labeled with Alexa Fluor 488 (Figure S10A). Although SPG20 did not bind to the GUVs before damage, laser-induced peroxidation triggered gradual recruitment of SPG20 to the GUV surface (Figure 6B). Like in cells, membrane recruitment was dependent on the lipid-packing sensing residues in the SC domain because the SPG20 8xV mutant did not detectibly bind to GUVs even after 1 min of irradiation (Figures 6C and 6D). Interestingly, even after longer irradiation, fluorescent SPG20 did not enter the lumen of the GUV indicating that damage detection by SPG20 does not coincide with permeability of the membrane for proteins. For further dissection, we tested the individual helices of the SC domain alone, fused to maltose-binding protein (MBP) (Figures S10B–S10F). Of note, helix 1 alone was sufficient to bind specifically to irradiated GUVs, whereas binding was not detected for any of the other 3 individual helices under the given conditions. This does not exclude that helices 2, 3, or 4 bind cooperatively with the other helices. Nevertheless, we confirmed in cells a prime role of helix 1 in damage-sensing by a set of six mutations to valine exclusively in helix 1 (H1–6xV), which largely reduced SPG20 recruitment to damaged lysosomes (Figures S10G–S10I). To independently demonstrate that SPG20 senses compromised lipid packing, we introduced lipid-packing defects by incorporation of the conical lipid dioleoyl glycerol (DOG) into the GUVs rather than inducing peroxidation. SPG20 specifically bound to DOG-containing GUVs, and this was again dependent on the bulky hydrophobic residues (Figures 6E and 6F). These results demonstrate that the SC domain of SPG20 directly senses lipid-packing defects, including those caused by lipid peroxidation (Figure 6G).

DISCUSSION

A key question in the cellular defense against LMP is how and based on what molecular cue the decision is made between the dramatically opposing response outcomes of repair and lysophagy. This decision has to be taken early and quickly in order to protect cells. Previous findings implicate exposure of luminal glycans to cytosolic components as a decisive driver for lysophagy.[6,7,24,25] Of note, glycan exposure requires extensive damage with formation of larger pores and bursts of the limiting membrane that cause permeability for proteins, consistent with our finding that Gal3 translocation occurs at higher concentrations of LLOMe than those required for SPG20. Thus, glycan detection is a strong cue for lysophagy initiation and likely most relevant when endolysosomes are fully and rapidly ruptured, for example, during bacterial infection.[6,7,43]

Our work presented here identifies lipid-packing defects that are sensed at the cytosolic side of permeabilized lysosomes as a critical cue for the initiation of lysophagy. This allows detection and isolation of compromised lysosomes before they burst and cause further damage to the cell. A damage signal emanating from the cytosolic leaflet of the limiting membrane is in line with the fact that damaged lysosomes can be subjected to lysophagy when they are topologically intact.[36,48] Lipid-packing defects occur, or are predicted to form, in membranes in patho-physiologically relevant conditions such as by lipid peroxidation, disease-associated changes of lipid compositions, or exposure to membranolytic agents.[8,43,44,49] We show here that SPG20 senses these defects with bulky hydrophobic amino acids in the amphipathic helices of the SPG20 SC domain, a structural feature that has previously mostly been linked to detection of membrane curvature. Helix 1 of the SC domain seems to play a prime role in the sensing. To what extent and in what order the other helices bind the membrane, and whether this involves opening of the predicted helical bundle needs to be determined in the future. It is possible that the sensing of damage-induced lipid-packing defects uncovered here is a more general principle for recruitment of additional autophagy regulators that bind membranes.[50]

Our data further reveal how detection of lipid-packing defects in the cytosolic leaflet by SPG20 triggers lysophagy initiation. We show that SPG20 binding of the lysosomal membrane recruits and activates the ubiquitin ligase ITCH. This induces ITCH-mediated K63 ubiquitylation of proteins on the topologically relevant cytosolic side, which can then directly recruit autophagy receptors to initiate lysophagy.

In lysosomal damage events, the ESCRT machinery is recruited quickly and sensitively by Ca^{2+} efflux, which is triggered through activation of Ca^{2+} channels even at minor damage.[10] It is therefore likely a default response to most damage to initiate repair. We show here that, when repair fails and damage increases in individual lysosomes, SPG20 interacts

(E) Quantification of (D).

(F) Positions of bulky hydrophobic residues replaced by valine in the indicated SPG20 variants. Structure predicted by AlphaFold.

(G) Translocation of SPG20 and recruitment of ITCH to damaged lysosomes depends on bulky hydrophobic residues in the SC domain of SPG20. SPG20 KO cells expressing GFP-tagged versions of SPG20 wt, SPG20 8xV, or SPG20 8xV fused to the ALPS motif of ARFGAP1 (8xV-ALPS^{ARFGAP1}) were mock or LLOMe-treated and costained for ITCH and LAMP1 (not shown here). See Figure S8H for control treatments.

(H) Quantification of (G).

Statistics: (B, E, and H) n = 3 biologically independent experiments with >20 cells quantified per condition. (B) Lines indicate median. (E and H) Error bars, SD. (B) Two-way ANOVA with Sidak's multiple comparison test. (E) Mixed-effects analysis with Tukey's multiple comparison test. (H) Two-way ANOVA with Tukey's multiple comparison test. Scale bars: 5 μm in (A) and 10 μm in (D) and (G).

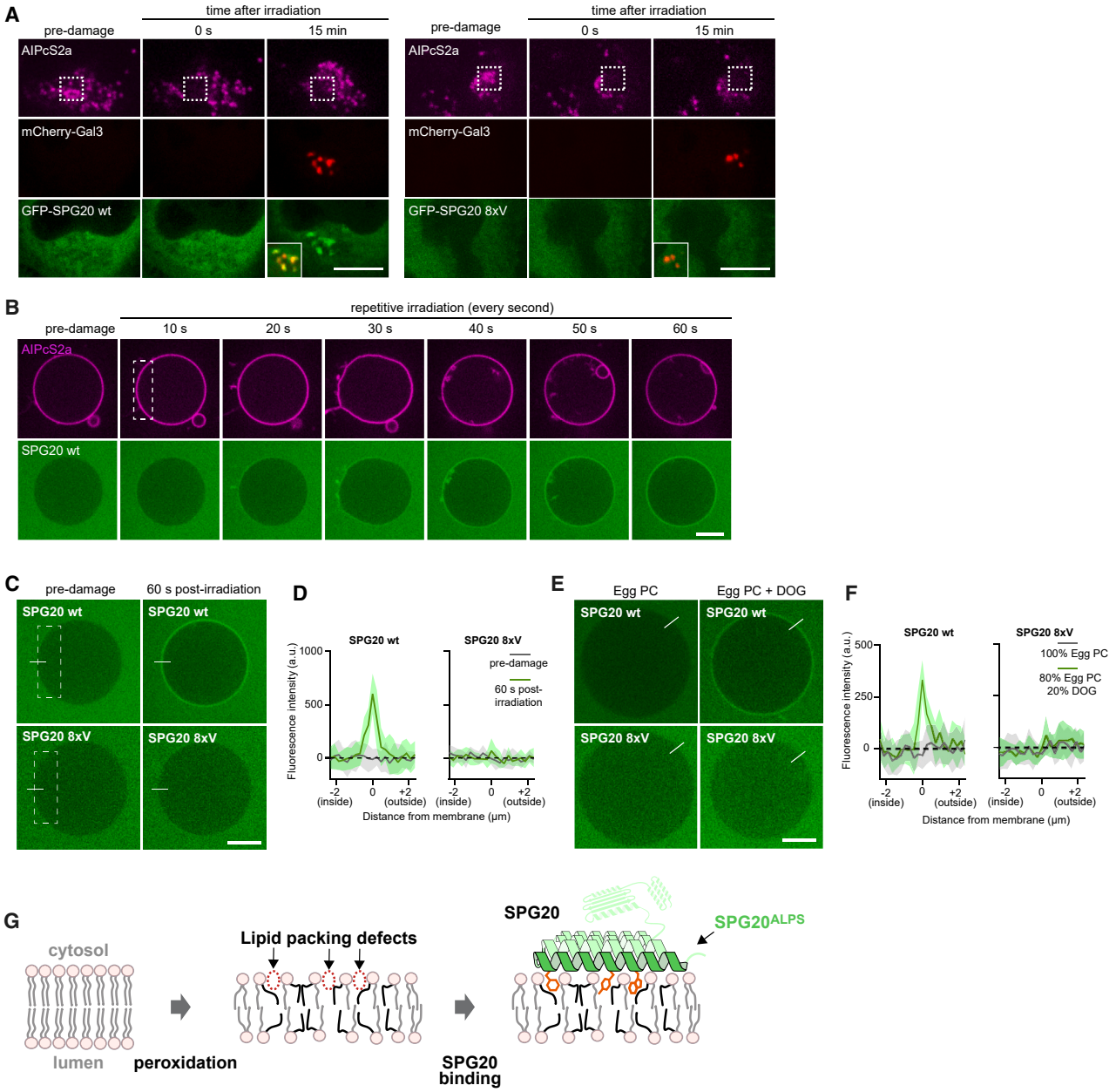

Figure 6. SPG20 detects lipid-packing defects induced by lipid peroxidation

(A) Lysosomes of cells expressing SPG20 WT or the 8xV mutant along with mCherry-Gal3 were loaded with the photosensitizer AlPcS2a. Indicated areas were laser-irradiated to induce lipid peroxidation. Translocation of Gal3 and SPG20 was followed over 15 min in live cells.

(B) GUVs were incorporated with photosensitizer and irradiated repetitively at the indicated area in the presence of SPG20 wild type. Note typical peroxidation-associated membrane deformations over time and GUV binding of SPG20 wild type.

(C) GUVs with incorporated photosensitizer were incubated with purified and Alexa488-labeled SPG20 WT or 8xV mutant for 15 min followed by laser irradiation in the indicated area.

(D) Fluorescence intensity profile before and after radiation along indicated line in (C).

(E) Direct binding of SPG20 to lipid-packing defects. Giant unilamellar vesicles (GUVs) were generated without or with conical lipid DOG that induces lipid-packing defects. GUVs were incubated with purified Alexa488-labeled SPG20 wild type or 8xV mutant.

(F) Quantification of (E) as in (D).

(G) Model of how SPG20 detects lipid-packing defects associated with lipid peroxidation.

Statistics: (D) Fluorescence intensity profile of SPG20 WT and 8xV was quantified for 10 GUVs. (F) 10 GUVs from 2 independent experiments were used for quantification. (D and F) Error bands, SD. Scale bars: 5 in (A) and 10 μm in (B), (C), and (E).

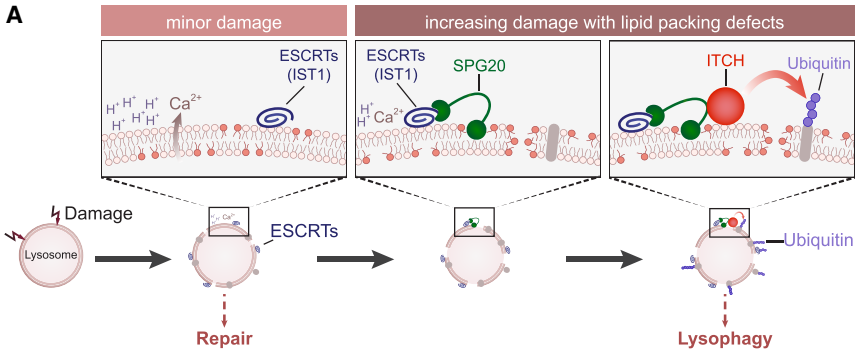

Figure 7. Model

(A) At lysosomes with minor membrane damage, Ca^{2+} is released and recruits the ESCRT machinery including IST1. If damage increases, SPG20 detects lipid-packing defects and binds IST1. SPG20 recruits and activates ITCH that ubiquitylates membrane-associated proteins to initiate lysophagy. Damage detection by SPG20 does not require permeability of the membrane for proteins.

with the ESCRT protein IST1 through the MIT domain in SPG20 while binding lipid perturbations with the SPG20 SC domain. We therefore posit that SPG20 is recruited by coincidence detection of both features and then recruits ITCH for lysophagy initiation (Figure 7). In cases in which damage rapidly progresses with disintegration of the membrane and exposure of glycoproteins and glycolipids, glycan-triggered responses will be quickly elicited and may dominate. By contrast, sensing lipid-packing defects by the SPG20-ITCH pathway is an early triaging cue for lysophagy initiation at lower damage levels and slowly progressing stress conditions, for example, during conditions that are associated with lipid alterations.

SPG20 was recently also reported to mediate lipophagy, the selective autophagy of lipid droplets.[34] Intriguingly, lipophagy was shown to not require ubiquitylation.[34] By contrast, lysophagy depends on ubiquitylation.[20] Consistent with that, we show that, during lysophagy, SPG20 binds and activates the ubiquitin ligase ITCH, and that ITCH and its interaction with SPG20 are essential for efficient lysophagy. Moreover, SPG20 is only recruited to lysosomes by damage-induced lipid-packing defects and binds ESCRT proteins that are absent on lipid droplets. Therefore, during lysophagy, the role of SPG20 is embedded in more complex levels of regulation than in lipophagy. The SPG20 SC domain was also proposed to have lipid transfer activity even though it does not have structural features of known lipid transfer domains.[51] Although we cannot exclude lipid transfer by SPG20 during the lysosomal damage response, we show that the role of SPG20 in this process relies on damage detection by the SC domain and is mediated by activation of ubiquitylation. Given that mutations in SPG20 cause Troyer syndrome,[52] a hereditary spastic paraplegia associated with distal amyotrophy and degeneration of motoneurons, our findings highlight the potential relevance of lysosomal maintenance and damage response, along with lipophagy, for counteracting neurodegeneration.

Limitations of the study

Due to the fact that our data were gathered and validated in human tissue culture cells, the implications of our findings for cellular homeostasis and signaling need to be tested for cell types and developmental stages of interest in organismal models.

STAR★METHODS

Detailed methods are provided in the online version of this paper and include the following:

- KEY RESOURCES TABLE
- RESOURCE AVAILABILITY
  - Lead contact
  - Materials availability
  - Data and code availability
- EXPERIMENTAL MODEL AND STUDY PARTICIPANT DETAILS
  - Cell lines
- METHOD DETAILS
  - Reagents and cell treatments
  - RNA isolation and reverse transcription
  - Plasmids
  - siRNA knockdown
  - Cell lysis and co-immunoprecipitation
  - Antibodies
  - Western blotting
  - Immunofluorescence staining and confocal microscopy
  - Live cell microscopy and photodamage
  - Structured Illumination Microscopy (SIM)
  - Lysophagy assay using TMEM192-mKeima cell line
  - Protein expression, purification, and labelling
  - Formation of GUVs
  - GUV microscopy and in vitro SPG20 binding assay
  - Image analysis and post-processing
  - DiGly proteomics
- QUANTIFICATION AND STATISTICAL ANALYSIS

SUPPLEMENTAL INFORMATION

Supplemental information can be found online at https://doi.org/10.1016/j.molcel.2024.02.029.

ACKNOWLEDGMENTS

We acknowledge the use of equipment and the support from the Imaging Center Campus Essen (ICCE) and specifically thank J. Koch for his help. We thank H. Stenmark for providing the PI4K2A knockout cell line and A. Hyman for CHMP4B-GFP cells. This work was supported by a joint grant of the Deutsche Forschungsgemeinschaft (DFG, German Research Foundation) to H.M. and C.B. (Project-ID 447112704). In addition, H.M. and N.S. were supported by

the DFG Collaborative Research Center 1430 (Project-ID 424228829), and C.B. by the DFG Munich Cluster for Systems Neurology (EXC 2145 SyNergy, ID 390857198) and the DFG Collaborative Research Center 1177 (ID 259130777). Microscopes were funded by the DFG – Project-IDs 397277702 and 496847469. S.P. is supported by the Associazione Italiana per la Ricerca sul Cancro (AIRC-IG#IG19875) and the Worldwide Cancer Research (19-0003).

AUTHOR CONTRIBUTIONS

H.M. conceived the study, designed the research plan, and wrote the manuscript. P.G., B.K., and G.R. performed most cell-based experiments, microscopy, and related analysis. B.K. performed GUV approaches. J.v.d.B. helped with biochemistry. N.S. helped with microscopy. S.L. and C.B. performed mass spectrometry including related cell treatments and analysis, as well as PI4K2A KO experiment. E.M. and S.P. provided NEDD4-like ligase constructs and advised. P.G. and B.K. prepared figures. All authors approved of the final version of the manuscript.

DECLARATION OF INTERESTS

The authors declare no competing interests.

Received: October 25, 2023
Revised: January 30, 2024
Accepted: February 27, 2024
Published: March 18, 2024

REFERENCES

1. Ballabio, A., and Bonifacino, J.S. (2020). Lysosomes as dynamic regulators of cell and organismal homeostasis. Nat. Rev. Mol. Cell Biol. *21*, 101–118.
2. Papadopoulos, C., and Meyer, H. (2017). Detection and Clearance of Damaged Lysosomes by the Endo-Lysosomal Damage Response and Lysophagy. Curr. Biol. *27*, R1330–R1341.
3. Wang, F., Gómez-Sintes, R., and Boya, P. (2018). Lysosomal membrane permeabilization and cell death. Traffic *19*, 918–931.
4. Logan, T., Simon, M.J., Rana, A., Cherf, G.M., Srivastava, A., Davis, S.S., Low, R.L.Y., Chiu, C.L., Fang, M., Huang, F., et al. (2021). Rescue of a lysosomal storage disorder caused by Grn loss of function with a brain penetrant progranulin biologic. Cell *184*, 4651–4668.e25.
5. Gabandé-Rodríguez, E., Pérez-Cañamás, A., Soto-Huelin, B., Mitroi, D.N., Sánchez-Redondo, S., Martínez-Sáez, E., Venero, C., Peinado, H., and Ledesma, M.D. (2019). Lipid-induced lysosomal damage after demyelination corrupts microglia protective function in lysosomal storage disorders. EMBO J. *38*, e99553.
6. Thurston, T.L., Wandel, M.P., von Muhlinen, N., Foeglein, A., and Randow, F. (2012). Galectin 8 targets damaged vesicles for autophagy to defend cells against bacterial invasion. Nature *482*, 414–418.
7. Chauhan, S., Kumar, S., Jain, A., Ponpuak, M., Mudd, M.H., Kimura, T., Choi, S.W., Peters, R., Mandell, M., Bruun, J.A., et al. (2016). TRIMs and Galectins Globally Cooperate and TRIM16 and Galectin-3 Co-direct Autophagy in Endomembrane Damage Homeostasis. Dev. Cell *39*, 13–27.
8. Petersen, N.H., Olsen, O.D., Groth-Pedersen, L., Ellegaard, A.M., Bilgin, M., Redmer, S., Ostenfeld, M.S., Ulanet, D., Dovmark, T.H., Lønborg, A., et al. (2013). Transformation-associated changes in sphingolipid metabolism sensitize cells to lysosomal cell death induced by inhibitors of acid sphingomyelinase. Cancer Cell *24*, 379–393.
9. Gupta, S., Yano, J., Mercier, V., Htwe, H.H., Shin, H.R., Rademaker, G., Cakir, Z., Ituarte, T., Wen, K.W., Kim, G.E., et al. (2021). Lysosomal retargeting of Myoferlin mitigates membrane stress to enable pancreatic cancer growth. Nat. Cell Biol. *23*, 232–242.
10. Skowyra, M.L., Schlesinger, P.H., Naismith, T.V., and Hanson, P.I. (2018). Triggered recruitment of ESCRT machinery promotes endolysosomal repair. Science *360*, eaar5078.
11. Radulovic, M., Schink, K.O., Wenzel, E.M., Nähse, V., Bongiovanni, A., Lafont, F., and Stenmark, H. (2018). ESCRT-mediated lysosome repair precedes lysophagy and promotes cell survival. EMBO J. *37*, e99753.
12. Zoncu, R., and Perera, R.M. (2022). Built to last: lysosome remodeling and repair in health and disease. Trends Cell Biol. *32*, 597–610.
13. Yang, H., and Tan, J.X. (2023). Lysosomal quality control: molecular mechanisms and therapeutic implications. Trends Cell Biol. *33*, 749–764.
14. Niekamp, P., Scharte, F., Sokoya, T., Vittadello, L., Kim, Y., Deng, Y., Südhoff, E., Hilderink, A., Imlau, M., Clarke, C.J., et al. (2022). Ca(2+)-activated sphingomyelin scrambling and turnover mediate ESCRT-independent lysosomal repair. Nat. Commun. *13*, 1875.
15. Radulovic, M., Wenzel, E.M., Gilani, S., Holland, L.K., Lystad, A.H., Phuyal, S., Olkkonen, V.M., Brech, A., Jäättelä, M., Maeda, K., et al. (2022). Cholesterol transfer via endoplasmic reticulum contacts mediates lysosome damage repair. EMBO J. *41*, e112677.
16. Tan, J.X., and Finkel, T. (2022). A phosphoinositide signalling pathway mediates rapid lysosomal repair. Nature *609*, 815–821.
17. Hoyer, M.J., Swarup, S., and Harper, J.W. (2022). Mechanisms Controlling Selective Elimination of Damaged Lysosomes. Curr. Opin. Physiol. *29*.
18. Vargas, J.N.S., Hamasaki, M., Kawabata, T., Youle, R.J., and Yoshimori, T. (2023). The mechanisms and roles of selective autophagy in mammals. Nat. Rev. Mol. Cell Biol. *24*, 167–185.
19. Yim, W.W., and Mizushima, N. (2020). Lysosome biology in autophagy. Cell Discov. *6*, 6.
20. Eapen, V.V., Swarup, S., Hoyer, M.J., Paulo, J.A., and Harper, J.W. (2021). Quantitative proteomics reveals the selectivity of ubiquitin-binding autophagy receptors in the turnover of damaged lysosomes by lysophagy. eLife *10*, e72328.
21. Fujita, N., Morita, E., Itoh, T., Tanaka, A., Nakaoka, M., Osada, Y., Umemoto, T., Saitoh, T., Nakatogawa, H., Kobayashi, S., et al. (2013). Recruitment of the autophagic machinery to endosomes during infection is mediated by ubiquitin. J. Cell Biol. *203*, 115–128.
22. Papadopoulos, C., Kirchner, P., Bug, M., Grum, D., Koerver, L., Schulze, N., Poehler, R., Dressler, A., Fengler, S., Arhzaouy, K., et al. (2017). VCP/p97 cooperates with YOD1, UBXD1 and PLAA to drive clearance of ruptured lysosomes by autophagy. EMBO J. *36*, 135–150.
23. Kravić, B., Bionda, T., Siebert, A., Gahlot, P., Levantovsky, S., Behrends, C., and Meyer, H. (2022). Ubiquitin profiling of lysophagy identifies actin stabilizer CNN2 as a target of VCP/p97 and uncovers a link to HSPB1. Mol. Cell *82*, 2633–2649.e7.
24. Liu, E.A., Schultz, M.L., Mochida, C., Chung, C., Paulson, H.L., and Lieberman, A.P. (2020). Fbxo2 mediates clearance of damaged lysosomes and modifies neurodegeneration in the Niemann-Pick C brain. JCI Insight *5*, e136676.
25. Yoshida, Y., Yasuda, S., Fujita, T., Hamasaki, M., Murakami, A., Kawawaki, J., Iwai, K., Saeki, Y., Yoshimori, T., Matsuda, N., and Tanaka, K. (2017). Ubiquitination of exposed glycoproteins by SCFFBXO27 directs damaged lysosomes for autophagy. Proc. Natl. Acad. Sci. USA *114*, 8574–8579.
26. Koerver, L., Papadopoulos, C., Liu, B., Kravic, B., Rota, G., Brecht, L., Veenendaal, T., Polajnar, M., Bluemke, A., Ehrmann, M., et al. (2019). The ubiquitin-conjugating enzyme UBE2QL1 coordinates lysophagy in response to endolysosomal damage. EMBO Rep. *20*, e48014.
27. Eastman, S.W., Yassaee, M., and Bieniasz, P.D. (2009). A role for ubiquitin ligases and Spartin/SPG20 in lipid droplet turnover. J. Cell Biol. *184*, 881–894.
28. Fajner, V., Maspero, E., and Polo, S. (2017). Targeting HECT-type E3 ligases - insights from catalysis, regulation and inhibitors. FEBS Lett. *591*, 2636–2647.

29. Thiele, D.L., and Lipsky, P.E. (1990). Mechanism of L-leucyl-L-leucine methyl ester-mediated killing of cytotoxic lymphocytes: dependence on a lysosomal thiol protease, dipeptidyl peptidase I, that is enriched in these cells. Proc. Natl. Acad. Sci. USA *87*, 83–87.

30. Lee, J.H., McBrayer, M.K., Wolfe, D.M., Haslett, L.J., Kumar, A., Sato, Y., Lie, P.P., Mohan, P., Coffey, E.E., Kompella, U., et al. (2015). Presenilin 1 Maintains Lysosomal Ca(2+) Homeostasis via TRPML1 by Regulating vATPase-Mediated Lysosome Acidification. Cell Rep. *12*, 1430–1444.

31. Shima, T., Ogura, M., Matsuda, R., Nakamura, S., Jin, N., Yoshimori, T., and Kuma, A. (2023). The TMEM192-mKeima probe specifically assays lysophagy and reveals its initial steps. J. Cell Biol. *222*.

32. Renvoisé, B., Parker, R.L., Yang, D., Bakowska, J.C., Hurley, J.H., and Blackstone, C. (2010). SPG20 protein spartin is recruited to midbodies by ESCRT-III protein Ist1 and participates in cytokinesis. Mol. Biol. Cell *21*, 3293–3303.

33. Joshi, D.C., and Bakowska, J.C. (2011). SPG20 protein spartin associates with cardiolipin via its plant-related senescence domain and regulates mitochondrial Ca2+ homeostasis. PLoS One *6*, e19290.

34. Chung, J., Park, J., Lai, Z.W., Lambert, T.J., Richards, R.C., Zhang, J., Walther, T.C., and Farese, R.V., Jr. (2023). The Troyer syndrome protein spartin mediates selective autophagy of lipid droplets. Nat. Cell Biol. *25*, 1101–1110.

35. Ulmschneider, M.B., Smith, J.C., and Ulmschneider, J.P. (2010). Peptide partitioning properties from direct insertion studies. Biophys. J. *98*, L60–L62.

36. Repnik, U., Borg Distefano, M., Speth, M.T., Ng, M.Y.W., Progida, C., Hoflack, B., Gruenberg, J., and Griffiths, G. (2017). L-leucyl-L-leucine methyl ester does not release cysteine cathepsins to the cytosol but inactivates them in transiently permeabilized lysosomes. J. Cell Sci. *130*, 3124–3140.

37. Heerklotz, H. (2008). Interactions of surfactants with lipid membranes. Q. Rev. Biophys. *41*, 205–264.

38. Antonny, B. (2011). Mechanisms of membrane curvature sensing. Annu. Rev. Biochem. *80*, 101–123.

39. Pinot, M., Vanni, S., Pagnotta, S., Lacas-Gervais, S., Payet, L.A., Ferreira, T., Gautier, R., Goud, B., Antonny, B., and Barelli, H. (2014). Lipid cell biology. Polyunsaturated phospholipids facilitate membrane deformation and fission by endocytic proteins. Science *345*, 693–697.

40. Vanni, S., Vamparys, L., Gautier, R., Drin, G., Etchebest, C., Fuchs, P.F., and Antonny, B. (2013). Amphipathic lipid packing sensor motifs: probing bilayer defects with hydrophobic residues. Biophys. J. *104*, 575–584.

41. Prévost, C., Sharp, M.E., Kory, N., Lin, Q., Voth, G.A., Farese, R.V., Jr., and Walther, T.C. (2018). Mechanism and Determinants of Amphipathic Helix-Containing Protein Targeting to Lipid Droplets. Dev. Cell *44*, 73–86.e4.

42. Hung, Y.H., Chen, L.M., Yang, J.Y., and Yang, W.Y. (2013). Spatiotemporally controlled induction of autophagy-mediated lysosome turnover. Nat. Commun. *4*, 2111.

43. Bour, A., Kruglik, S.G., Chabanon, M., Rangamani, P., Puff, N., and Bonneau, S. (2019). Lipid Unsaturation Properties Govern the Sensitivity of Membranes to Photoinduced Oxidative Stress. Biophys. J. *116*, 910–920.

44. Van der Paal, J., Neyts, E.C., Verlackt, C.C.W., and Bogaerts, A. (2016). Effect of lipid peroxidation on membrane permeability of cancer and normal cells subjected to oxidative stress. Chem. Sci. *7*, 489–498.

45. Shi, X., Mao, Y., Daniel, L.N., Saffiotti, U., Dalal, N.S., and Vallyathan, V. (1994). Silica radical-induced DNA damage and lipid peroxidation. Environ. Health Perspect. *102* (suppl 10), 149–154.

46. Bhardwaj, M., Lee, J.J., Versace, A.M., Harper, S.L., Goldman, A.R., Crissey, M.A.S., Jain, V., Singh, M.P., Vernon, M., Aplin, A.E., et al. (2023). Lysosomal lipid peroxidation regulates tumor immunity. J. Clin. Invest. *133*.

47. Sankhagowit, S., Wu, S.H., Biswas, R., Riche, C.T., Povinelli, M.L., and Malmstadt, N. (2014). The dynamics of giant unilamellar vesicle oxidation probed by morphological transitions. Biochim. Biophys. Acta *1838*, 2615–2624.

48. Maejima, I., Takahashi, A., Omori, H., Kimura, T., Takabatake, Y., Saitoh, T., Yamamoto, A., Hamasaki, M., Noda, T., Isaka, Y., and Yoshimori, T. (2013). Autophagy sequesters damaged lysosomes to control lysosomal biogenesis and kidney injury. EMBO J. *32*, 2336–2347.

49. Vamparys, L., Gautier, R., Vanni, S., Bennett, W.F., Tieleman, D.P., Antonny, B., Etchebest, C., and Fuchs, P.F. (2013). Conical lipids in flat bilayers induce packing defects similar to that induced by positive curvature. Biophys. J. *104*, 585–593.

50. de la Ballina, L.R., Munson, M.J., and Simonsen, A. (2020). Lipids and Lipid-Binding Proteins in Selective Autophagy. J. Mol. Biol. *432*, 135–159.

51. Wan, N., Hong, Z., Parson, M.A.H., Korfhage, J.L., Burke, J.E., Melia, T.J., and Reinisch, K.M. (2024). Spartin-mediated lipid transfer facilitates lipid droplet turnover. Proc. Natl. Acad. Sci. USA *121*, e2314093121.

52. Patel, H., Cross, H., Proukakis, C., Hershberger, R., Bork, P., Ciccarelli, F.D., Patton, M.A., McKusick, V.A., and Crosby, A.H. (2002). SPG20 is mutated in Troyer syndrome, an hereditary spastic paraplegia. Nat. Genet. *31*, 347–348.

53. Poser, I., Sarov, M., Hutchins, J.R., Hériché, J.K., Toyoda, Y., Pozniakovsky, A., Weigl, D., Nitzsche, A., Hegemann, B., Bird, A.W., et al. (2008). BAC TransgeneOmics: a high-throughput method for exploration of protein function in mammals. Nat. Methods *5*, 409–415.

54. Ishihara, T., Tsuda, H., Hotta, A., Kozaki, K., Yoshida, A., Noh, J.Y., Ito, K., Imoto, I., and Inazawa, J. (2008). ITCH is a putative target for a novel 20q11.22 amplification detected in anaplastic thyroid carcinoma cells by array-based comparative genomic hybridization. Cancer Sci. *99*, 1940–1949.

55. Malik, R., Soh, U.J., Trejo, J., and Marchese, A. (2012). Novel roles for the E3 ubiquitin ligase atrophin-interacting protein 4 and signal transduction adaptor molecule 1 in G protein-coupled receptor signaling. J. Biol. Chem. *287*, 9013–9027.

56. Bakowska, J.C., Jupille, H., Fatheddin, P., Puertollano, R., and Blackstone, C. (2007). Troyer syndrome protein spartin is mono-ubiquitinated and functions in EGF receptor trafficking. Mol. Biol. Cell *18*, 1683–1692.

57. Woelk, T., Oldrini, B., Maspero, E., Confalonieri, S., Cavallaro, E., Di Fiore, P.P., and Polo, S. (2006). Molecular mechanisms of coupled monoubiquitination. Nat. Cell Biol. *8*, 1246–1254.

58. Stirling, D.R., Swain-Bowden, M.J., Lucas, A.M., Carpenter, A.E., Cimini, B.A., and Goodman, A. (2021). CellProfiler 4: improvements in speed, utility and usability. BMC Bioinformatics *22*, 433.

59. Cox, J., and Mann, M. (2008). MaxQuant enables high peptide identification rates, individualized p.p.b.-range mass accuracies and proteome-wide protein quantification. Nat. Biotechnol. *26*, 1367–1372.

60. Cox, J., Neuhauser, N., Michalski, A., Scheltema, R.A., Olsen, J.V., and Mann, M. (2011). Andromeda: a peptide search engine integrated into the MaxQuant environment. J. Proteome Res. *10*, 1794–1805.

61. Hülsmann, J., Kravic, B., Weith, M., Gstaiger, M., Aebersold, R., Collins, B.C., and Meyer, H. (2018). AP-SWATH Reveals Direct Involvement of VCP/p97 in Integrated Stress Response Signaling Through Facilitating CReP/PPP1R15B Degradation. Mol. Cell. Proteomics *17*, 1295–1307.

62. Ritz, D., Vuk, M., Kirchner, P., Bug, M., Schütz, S., Hayer, A., Bremer, S., Lusk, C., Baloh, R.H., Lee, H., et al. (2011). Endolysosomal sorting of ubiquitinated caveolin-1 is regulated by VCP/p97 and UBXD1 and impaired by VCP disease mutations. Nat. Cell Biol. *13*, 1116–1123.

63. Tanaka, A., Cleland, M.M., Xu, S., Narendra, D.P., Suen, D.F., Karbowski, M., and Youle, R.J. (2010). Proteasome and p97 mediate mitophagy and degradation of mitofusins induced by Parkin. J. Cell Biol. *191*, 1367–1380.

64. Weinberger, A., Tsai, F.C., Koenderink, G.H., Schmidt, T.F., Itri, R., Meier, W., Schmatko, T., Schröder, A., and Marques, C. (2013). Gel-assisted formation of giant unilamellar vesicles. Biophys. J. *105*, 154–164.

65. Cutler, K.J., Stringer, C., Lo, T.W., Rappez, L., Stroustrup, N., Brook Peterson, S., Wiggins, P.A., and Mougous, J.D. (2022). Omnipose: a high-precision morphology-independent solution for bacterial cell segmentation. Nat. Methods *19*, 1438–1448.

66. Fiskin, E., Bionda, T., Dikic, I., and Behrends, C. (2016). Global Analysis of Host and Bacterial Ubiquitinome in Response to Salmonella Typhimurium Infection. Mol. Cell *62*, 967–981.

67. Villén, J., and Gygi, S.P. (2008). The SCX/IMAC enrichment approach for global phosphorylation analysis by mass spectrometry. Nat. Protoc. *3*, 1630–1638.

68. Rappsilber, J., Ishihama, Y., and Mann, M. (2003). Stop and go extraction tips for matrix-assisted laser desorption/ionization, nanoelectrospray, and LC/MS sample pretreatment in proteomics. Anal. Chem. *75*, 663–670.

STAR★METHODS

KEY RESOURCES TABLE

REAGENT or RESOURCE	SOURCE	IDENTIFIER
Antibodies		
Rat monoclonal anti-Gal3 (IF, 1:500)	Santa Cruz Biotechnology	Cat#sc-23938; RRID:AB_627658
Rabbit monoclonal anti-LAMP1 (IF, 1:500)	Cell Signaling Technology	Cat#9091; RRID:AB_2687579
Mouse monoclonal anti-LAMP1 (IF, 1:500)	Santa Cruz Biotechnology	Cat#sc-20011 RRID:AB_626853
Rabbit polyclonal anti-SPG20 (IF, 1:500)	Thermo Fisher Scientific	Cat#PA5-65224; RRID:AB_2664013
Mouse monoclonal anti-SPG20 (IF, 1:500; WB, 1:1000)	Santa Cruz Biotechnology	Cat#sc-271888; RRID:AB_10709900
Rabbit polyclonal anti-LC3 (IF, 1:500; WB, 1:1000)	MBL	Cat#PM036; RRID:AB_2274121
Mouse monoclonal ITCH (IF, 1:500; WB, 1:1000)	BD Biosciences	Cat#611198; RRID:AB_398732
Rabbit polyclonal IST1 (IF, 1:500; WB, 1:5000)	Proteintech	Cat#51002-1-AP; RRID:AB_2130516
Mouse monoclonal IST1 (IF, 1:500)	Proteintech	Cat#66989-1-Ig; RRID:AB_2882306
Rabbit monoclonal K63-linkage specific polyubiquitin (D7A11) (IF, 1:500)	Cell Signaling Technology	Cat#5621; RRID:AB_10827985
Rabbit polyclonal p62 (IF, 1:500)	Sigma	Cat#P0067; RRID:AB_1841064
Rabbit polyclonal anti-TAX1BP1 (IF, 1:500; WB, 1:1000)	Sigma	Cat#HPA024432; RRID:AB_1857783
Mouse monoclonal anti-p97 (WB, 1:2000)	Santa Cruz Biotechnology	Cat#sc-57492; RRID:AB_793927
Mouse monoclonal anti-P4D1 (WB, 1:1000)	Cell Signaling Technology	Cat#3936; RRID:AB_331292
Mouse monoclonal anti-Tubulin (WB, 1:5000)	Sigma-Aldrich	Cat#T-5168; RRID:AB_477579
Rabbit polyclonal PI4K2A (WB, 1:1000)	Proteintech	Cat#15318-1-AP; RRID:AB_2268225
Rabbit polyclonal PLIN3 (TIP47) (IF, 1:500)	Proteintech	Cat#10694-1-AP; RRID:AB_2297252
Mouse monoclonal anti-GFP (WB, 1:10000)	Roche	Cat#11814460001; RRID:AB_390913
horseradish peroxidase (HRP)-conjugated goat anti-rabbit IgG (WB, 1:10000)	Biorad	Cat#170-6515; RRID:AB_11125142
horseradish peroxidase (HRP)-conjugated goat anti-mouse IgG (WB, 1:10000)	Biorad	Cat#1706516; RRID:AB_11125547
Alexa Fluor-conjugated goat anti-rabbit, Alexa Fluor™ 568 (IF, 1:500)	Invitrogen	Cat#A11011; RRID:AB_143157
Alexa Fluor-conjugated goat anti-rabbit, Alexa Fluor™ 488 (IF, 1:500)	Life technologies	Cat#A11034; RRID:AB_2576217
Alexa Fluor-conjugated goat anti-rabbit, Alexa Fluor™ 633 (IF, 1:500)	Thermo Fisher Scientific	Cat#A21071; RRID:AB_2535732
Alexa Fluor-conjugated goat anti-mouse, Alexa Fluor™ 488 (IF, 1:500)	Thermo Fisher Scientific	Cat#10696113
Alexa Fluor-conjugated goat anti-mouse, Alexa Fluor™ 594 (IF, 1:500)	Thermo Fisher Scientific	Cat#A-11032; RRID:AB_2534091
Alexa Fluor-conjugated goat anti-mouse, Alexa Fluor™ 633 (IF, 1:500)	Thermo Fisher Scientific	Cat#10246252
Alexa Fluor-conjugated goat anti-rat, Alexa Fluor™ 488 (IF, 1:500)	Thermo Fisher Scientific	Cat#A-11006; RRID:AB_2534074
Alexa Fluor-conjugated goat anti-rat, Alexa Fluor™ 568 (IF, 1:500)	Thermo Fisher Scientific	Cat#A-11077; RRID:AB_2534121

(*Continued on next page*)

Continued

REAGENT or RESOURCE	SOURCE	IDENTIFIER
Alexa Fluor-conjugated goat anti-rat, Alexa Fluor™ 633 (IF, 1:500)	Thermo Fisher Scientific	Cat#A-21094; RRID:AB_2535749
Bacterial and virus strains		
Escherichia coli BL21 (DE3)	New England Biolabs	Cat#C2527I
Escherichia coli XL1-Blue Competent Cells	Agilent	Cat#200249
Chemicals, peptides, and recombinant proteins		
DMEM	PAN-Biotech	Cat#P04-03590
DMEM/F12	PAN-Biotech	Cat#P04-41150
FBS	PAN-Biotech	Cat#P30-3306
DPBS	PAN-Biotech	Cat#P04-36500
Penicillin/Streptomycin	PAN-Biotech	Cat#P06-07100
Imaging medium	PAN-Biotech	Cat#P04-03591
Spodopan	PAN-Biotech	Cat#P04-850500
Trypsin-EDTA	PAN-Biotech	Cat#P10-23100
G-418 disulphate	PanReac AppliChem	Cat#A2167.0001
Puromycin	Sigma	Cat#P8833-100MG
L-Leucyl-L-Leucine methyl ester hydrobromide (LLOMe)	Sigma	Cat#L7393
ML-SA1	Merck Millipore	Cat#SML0627
Nano-SiO_2	Invivogen	Cat#tlrl-sio-2
DC661	MedChem Express	Cat#HY-111621
Chloroquine diphosphate salt	Merck/Sigma Aldrich	Cat#C6628-50G
AlPcS2a	Frontier Scientific	Cat#P40632
Egg PC	Avanti/Merck	Cat#840051P-500MG
16:0–18:1 PS (POPS)	Avanti/Merck	Cat#840034P-25MG
18:1 DG (DOG)	Avanti/Merck	Cat#800811C-25MG
Cholesterol	Avanti/Merck	Cat#700100P-200MG
TRIzol Reagent	Thermo Fisher Scientific	Cat#15596026
Complete EDTA-free Protease Inhibitor Cocktail	Roche	Cat#04693132001
SuperSignal West Pico Chemiluminescent substrate	Pierce	Cat#15669364
ECL Prime Western Blotting Detection Reagent	Amersham	Cat#12994780(RPN2236)
IPTG (Isopropyl-β-D-thiogalactopyranosid)	VWR	Cat#A1008.0100
Alexa Fluor™ 488 C5 Maleimid	Thermo Fisher Scientific	Cat#10593233
ProLong Gold	Thermo Fisher Scientific	Cat#P36930
Critical commercial assays		
BC Assay Protein Quantification Kit	VWR	Cat#733-1404
SuperScript II Reverse Transkriptase	Thermo Fisher Scientific	Cat#18064014
Oligo (dT) 12-18 Primer 0,5μg/μl	Thermo Fisher Scientific	Cat#18418012
Gibson Assembly Kit	Thermo Fisher Scientific	Cat#A46627
PTMScan® Ubiquitin Remnant Motif (K-ε-GG)	Cell Signaling Technology	Cat#5562
Deposited data		
Raw Western Blot and Microscopy Data, and Cell Profiler pipelines	This paper; Mendeley Data	Part 1: https://doi.org/10.17632/6kfbpr73w6.1 Part 2: https://doi.org/10.17632/3fjzxbr679.1 Part 3: https://doi.org/10.17632/988rrt5dk8.1 Part 4: https://doi.org/10.17632/8bjbtwc2fp.1 Part 5: https://doi.org/10.17632/pvz62pdt4n.1 Part 6: https://doi.org/10.17632/gdhpxjpsp5.1 Part 7: https://doi.org/10.17632/k5grf4464j.1 Part 8: https://doi.org/10.17632/mhzfnvnfws.1

(*Continued on next page*)

Continued

REAGENT or RESOURCE	SOURCE	IDENTIFIER
Mass Spectrometry Data	This paper; https://www.ebi.ac.uk/pride/archive	PXD039088
Experimental models: Cell lines		
Human: HeLa Kyoto	Prof. Shuh Narumiya (Kyoto University)	RRID:CVCL_1922
Human: U2OS	N/A	RRID:CVCL_0042
Human: ARPE19	ATCC	Cat#CRL-2302; RRID:CVCL_0145
Human: SH-SY5Y	N/A	RRID:CVCL_0019
Human: HeLa SPG20 KO	This paper	N/A
Human: HeLa ITCH KO	This paper	N/A
Human: HeLa SPG20 KO GFP-SPG20 wt	This paper	N/A
Human: HeLa SPG20 KO GFP-SPG20 ΔMIT	This paper	N/A
Human: HeLa TMEM192-mKeima	This paper	N/A
Human: HeLa YFP-ITCH	This paper	N/A
Human: HeLa CHMP4B-GFP	Poser et al.[53]	N/A
Human: HeLa PI4K2A KO	Radulovic et al.[15]	N/A
Insect: Sf9	Thermo Fisher Scientific	Cat# 11496015; RRID:CVCL_0549
Insect: High Five	Thermo Fisher Scientific	Cat#B85502; RRID:CVCL_C190
Oligonucleotides		
sgRNA ITCH (TGGACCAAGTCCTTACGTAG)	This paper	N/A
siITCH #1: 5' GGAGCAACAUCUGGAUUAAUA 3'	Ishihara et al.[54]; Microsynth	N/A
siITCH #2: 5′ GGUGACAAAGAGCCAACAGAG 3′	Malik et al.[55]; Microsynth	N/A
siSPG20 #1: 5' GGCAAGGAUUGGAAU GUGCAGCUAA 3'	Bakowska et al.[56]; Microsynth	N/A
siSPG20 #2: 5' GGGAATCACTTATACCA AAGCCTTA 3'	Microsynth	N/A
siSPG20 #3: 5' GAAGGAAGAAGCAAAGAACTA 3	Microsynth	N/A
siSPG20 #4: 5' GTTGTAGCAGCAAGTAGTGTT 3'	Microsynth	N/A
siSPG20 #5: 5' GTGGATTCTGCGGTCAATGTT 3'	Microsynth	N/A
siPI4K2A #1	Dharmacon	J-006770-06-0002
siPI4K2A #2	Dharmacon	J-006770-07-0002
siIST1: 5' CCAGUCAGAAGUGGCUGAGU UGAAA 3'	Renvoise et al.[32]; Microsynth	N/A
Recombinant DNA		
pDONR221-SPG20	This paper	N/A
pcDNA5 FRT/TO GFP-SPG20	This paper	N/A
peGFP C3-SPG20	This paper	N/A
peGFP C1-SPG20-1-418aa	This paper	N/A
peGFP C3-SPG20-PAAA	This paper	N/A
pcDNA5 FRT/TO GFP-SPG20-PAAA	This paper	N/A
pcDNA5 FRT/TO GFP-SPG20	This paper	N/A
pmCherry C2-Optn	This paper	N/A
peGFP C1-SPG20 SC domain	This paper	N/A
peGFP C3-SPG20-ΔMIT	This paper	N/A
peGFP C3-SPG20 8xV	This paper	N/A
peGFP C3-SPG20 23xV	This paper	N/A
peGFP C3-SPG20 6xV	This paper	N/A
peGFP C3-SPG20 H1-6xV	This paper	N/A
peGFP C2-IST1	This paper	N/A

(*Continued on next page*)

Continued

REAGENT or RESOURCE	SOURCE	IDENTIFIER
pmCherry N1-IST1	This paper	N/A
pCR3.1 YFP-ITCH	Woelk et al.[57]	N/A
pCR3.1-YFP-ITCH-CA mutant (C871A)	This paper	N/A
pcDNA3 TMEM192-mKeima	This paper	N/A
pmCherry C1-ARFGAP1-ALPS (137-237aa)	This paper	N/A
pmCherry C1-ARFGAP1-ALPS-SH mutant	This paper	N/A
pmCherry C1-Gal3	Addgene; Papadopoulos et al.[22]	Cat#85662; RRID:Addgene_85662
peGFP C1-HECW1	This paper	N/A
peGFP C1-HECW2	This paper	N/A
pCR3.1-YFP-WWP2	Woelk et al.[57]	N/A
peGFP-C1-NEDD4	Woelk et al.[57]	N/A
peGFP-C1-NEDD4L	Woelk et al.[57]	N/A
peGFP N1-GMAP210 (1-375aa)	This paper	N/A
peGFP C3-SPG20-8xV-ALPS^{ARFGAP1}	This paper	N/A
pmCherry C1-ITCH	This paper	N/A
pET28 MBP-Cys-SPG20_SC-H1	This paper	N/A
pET28 MBP-Cys-SPG20_SC-H2	This paper	N/A
pET28 MBP-Cys-SPG20_SC-H3	This paper	N/A
pET28 MBP-Cys-SPG20_SC-H4	This paper	N/A
pFL His-SPG20	This paper	N/A
pFL His-SPG20 8V	This paper	N/A
Software and algorithms		
Fiji	NIH	http://fiji.sc RRID:SCR_002285
Adobe Photoshop	Adobe Inc.	https://www.adobe.com/products/photoshop.html RRID:SCR_014199
Adobe Illustrator	Adobe Inc.	http://www.adobe.com/products/illustrator.html RRID:SCR_010279
Cell Profiler software 44 (4.2.5)	Broad Institute; Stirling et al.[58]	https://cellprofiler.org/ RRID:SCR_007358
Cell Profiler software 44 (2.1.1)	Broad Institute	https://cellprofiler.org/ RRID:SCR_007358
Leica Application Suite X	Leica Microsystems	https://www.leica-microsystems.com/products/microscope-software/details/product/leica-las-x-ls/ RRID:SCR_013673
Andor iQ	Oxford Instruments	http://www.andor.com/scientific-software/iq-live-cell-imaging-software RRID:SCR_014461
Excel (2021)	Microsoft Corporation	https://office.microsoft.com/excel
SoftMax Pro	Molecular Devices	RRID:SCR_014240
MaxQuant (1.6.0.1)	Cox and Mann[59]; Cox et al.[60]	RRID:SCR_014485
UCSF ChimeraX 1.6.1	UCSF Resource for Biocomputing, Visualization, and Informatics	UCSF ChimeraX https://www.rbvi.ucsf.edu/chimerax/ RRID:SCR_015872
GraphPad Prism 9.0	GraphPad Software (San Diego, USA)	www.graphpad.com RRID:SCR_002798

RESOURCE AVAILABILITY

Lead contact

Further information and requests for resources and reagents should be directed to and will be fulfilled by Hemmo Meyer (hemmo.meyer@uni-due.de).

Materials availability

Plasmids and cell lines generated in this study will be available upon request.

Data and code availability

- Original Western blot data, microscopy images and Cell Profiler pipelines used in this paper have been deposited at Mendeley Data and are publicly available as of the date of publication. The DOIs are listed in the key resources table. The mass spectrometry proteomics data have been deposited to the ProteomeXchange Consortium via the PRIDE partner repository (https://www.ebi.ac.uk/pride/archive/) with the dataset identifier PXD039088.
- This paper does not report original code.
- Any additional information required to reanalyze the data reported in this paper is available from the lead contact upon request.

EXPERIMENTAL MODEL AND STUDY PARTICIPANT DETAILS

Cell lines

Cells (HeLa Kyoto and U2OS) were cultured in Dulbecco's modified Eagle's medium (DMEM) or in DMEM:F12 medium (ARPE19, SH-SY5Y) supplemented with 10% fetal bovine serum (FBS, PAN-Biotech) and 1% Penicillin/Streptomycin (PAN-Biotech). Cells were grown in standard conditions, 37 °C and 5% CO_2. For generation of stable cell lines (YFP-ITCH or TMEM192-mKeima), HeLa Kyoto cells were transfected with circular pCR3.1 YFP-ITCH or pcDNA3 TMEM192-mKeima, respectively and cultured in DMEM containing 10% FBS, 1% Penicillin/Streptomycin and selection antibiotic G418 (500 μg/ml or 1 mg/ml). HeLa SPG20 KO cells were generated using Spartin Double Nickase Plasmid (Santa Cruz Biotechnology, sc-407769-NIC) according to manufacturer's instructions. Cell lines were not authenticated. HeLa CHMP4B-GFP cells were described before.[53] For generation of stable cell lines expressing GFP-SPG20 wt or ΔMIT, HeLa SPG20KO cells were transfected with circular peGFP C3-SPG20 wt or ΔMIT, respectively and cultured in DMEM containing 10% FBS, 1% Penicillin/Streptomycin and selection antibiotic G418 (1 mg/ml).

HeLa ITCH KO cells were generated using sgRNA (TGGACCAAGTCCTTACGTAG) against exon 4 of ITCH gene using CRISPR Cas9 technology to introduce a premature stop codon in exon 4. ITCH knockout was confirmed by Sanger sequencing following genomic PCR to amplify exon 4 of ITCH. The following primers were used to amplify exon 4 of ITCH from genomic DNA in order to confirm the knockout: 5'-GGCATTCAGATGTTTGTTGACCA-3' and 5'-AATAACTATAGTATAACTGGCACCGTAA-3'. For Sanger sequencing, 5'-GAATTCTACTGATGGGAATTTGGG-3' primer was used and deletion of exon 4 of ITCH gene was confirmed. The knockout was also confirmed on western blot (the minor ITCH isoform 3 which lacks exon 4 was still expressed in cells). HeLa PI4K2A knockout cells were kindly provided by Stenmark.[15]

METHOD DETAILS

Reagents and cell treatments

To induce lysosomal damage, cells were treated with L-Leucyl-L-Leucine methyl ester hydrobromide (LLOMe, Sigma) at 1 mM if not otherwise indicated. Chloroquine was used at 100 μM for indicated times. ML-SA1 (Merck Millipore; SML0627) was used at 25 μM. For silica-induced lysosomal damage, HeLa cells were treated with 50 μg/mL nano-SiO_2 (Invivogen, tlrl-sio-2). DC661 (MedChem Express, HY-111621) was used at 3 μM for 2 h.

RNA isolation and reverse transcription

Total RNA was isolated from HeLa cells using TRIzol reagent (Invitrogen) according to manufacturer's instructions. Complementary DNA (cDNA) was synthetized from 4 μg RNA using SuperScriptTM II Reverse Transcriptase (Invitrogen) according to manufacturer's instructions.

Plasmids

Human SPG20 cDNA was amplified from HeLa cDNA using the following oligos containing attB sites (5 '-GGGGACCA AGTTTGTACAAAAAAGCAGGCTTCatgGAGCAAGAGCCACAAA-3' and 5 '-GGGGACCACTTTGTACAAGAAAGCTGGGTCTCATT TATCTTTCTTCTTT-3') and subcloned into pDONR221 vector (Invitrogen) and then into pcDNA5 FRT/TO GFP vector (described before[61]) using the Gateway cloning system. pcDNA5 FRT/TO GFP-SPG20 was used as a template for amplification of SPG20 ORF using primers containing HindIII (5'-TATAAGCTTATGGAGCAAGAGCCACAAA-3 ') or BamHI (5'-TATGGATCCTCATT TATCTTTCTTCTTTGC-3 ') restriction sites and subcloned into peGFP C3 vector (Clontech). peGFP C1-SPG20-1-418aa and peGFP

C1-SPG20 SC domain were cloned by amplifying 1-418 residues and 418-666 residues of SPG20 ORF from peGFP C3-SPG20, respectively and subcloning into peGFP C1 using Gibson assembly. peGFP C3-SPG20-PAAA mutant was generated using HindIII and BamHI restriction sites containing primers to amplify SPG20-PAAA from pcDNA5 FRT/TO GFP-SPG20-PAAA vector (previously generated by PG) and subcloning into peGFP C3 vector. peGFP C3-SPG20-ΔMIT coding for SPG20 amino acids 108-666 was cloned by amplifying SPG20-ΔMIT from pcDNA5 FRT/TO GFP-SPG20 vector using primers containing HindIII (5 '- TAT AAGCTTCAGGAGGTGCCCAAGTTA-3 ') or BamHI (5 '-TATGGATCCTCATTTATCTTTCTTCTTTGC-3') restriction sites and subcloned into peGFP C3 vector. The specified bulky hydrophobic residues were mutated to valine in SPG20 8xV (W419, L438, I449, L456, F549, L556, I563 and I609), 6xV (W419, F549, W553, Y579, Y602 and Y628) and 23xV (W419, I427, W433, L438, I449, L456, I460, L477, L494, L509, L525, F549, W553, L556, I563, Y579, Y602, I604, I607, I609, M612, L624 and Y628) mutants and ordered as g-blocks DNA fragments (Integrated DNA Technologies) and introduced into peGFP C3-SPG20 amplified fragment (5 '-TCAGATAGTTGATAATTCTCAGAGGGAAAATCAAG-3' and 5'-TTCACTCTGTTCAGGTAATTCTTTTGGC-3') using Gibson assembly. SPG20 H1-6xV was also generated using Gibson assembly with the specified residues (W419V, W433V, L438V, I444V, I449V and L456V) mutated to valine and introduced into peGFP C3-SPG20 as described above.

peGFP C2-IST1 was generated by amplifying human IST1 from HeLa cDNA using following oligos containing EcoRI (5'-TATGAATTCATGCTGGGCTCTGGATTTA-3') or KpnI (5'-TATGGTACCCTATGTTTTCTTTTTCAGC-3') and subcloning into peGFP C2 vector (Clontech). Human IST1 was subcloned into the pmCherry N1 vector using the following primers (5'-TCCACCATGGTGAG CAAGGGCGAG-3' and 5'- GCGACCGGTGGATCCCGG-3') for site directed mutagenesis.

pmCherry C1-ARFGAP1-ALPS coding for residues 137-237 of human ARFGAP1 (isoform1) and pmCherry C1-ARFGAP1-ALPS-SH mutant (where the following bulky hydrophobic residues were mutated to valine: F199, Y208, W211, F214 and F221 (previously described in [41]) were cloned using codon optimised ARFGAP1-ALPS or ARFGAP1-ALPS SH gBlock (IDT) with KpnI and BamHI restriction sites into pmCherry C1 vector. GMAP210 ALPS coding for residues 1-375 of human GMAP210 was purchased as a gBlock (IDT) and cloned into peGFP N1 by restriction digestion using XhoI and HindIII.

The peGFP C3-SPG20-ARFGAP1-ALPS fusion 8V plasmid was cloned using following primers:

peGFP C3-SPG20 8xV-ARFGAP1-ALPS: 5'- TCGGCTCTCAGGCAAGCTAATGAGGATCCACCGGATCTAG-3', 5'- CTAGATCCG GTGGATCCTCATTAGCTTGCCTGAGAGCC-3', 5'- GGCAAGGTCCTAGGTTGGGGAAGCTTGAGCTCGAGATCTGAGTATTTATCTT TCTTCTTTGCCTCC-3' and 5'- AGGCAAAGAAGAAAGATAAATACTCAGATCTCGAGCTCAAGCTTCCCCAACCTAGGACCTTG-3'.

pRK-Myc-SMURF1 (human; Addgene; #13676) was used as a template to subclone SMURF1 into peGFP C1 vector using the following primers: 5'-GCTCAA GCT TCG AAT TCCATGTCGAACCCCG-3' and 5'-CGGGGTTCGACATGGAATTCGAAGCTT GAGC-3'.

The complete CDS of HECW1 (cDNA FLJ58788) was amplified with the following oligos: 5'-CGCGGATCCATGCTGCTG CACCTGTGTAGTGTG-3' and 5'-CCGCGGATCCTCACTCAAGTCCAAAGGTGCTGGTTTCC-3' and cloned into peGFP-C1 vector using BamHI site. The complete cds of HECW2 (cDNA clone MGC:150803 IMAGE:40125745) was amplified with the following oligos: 5'-CCGCTCGAGATGGCTAGTTCAGCCCGGGAG-3' and 5'-CCGCTCGAGTCACTCAAGTCCAAAAGTACTGG-3', and cloned into peGFP-C1 vector using SalI site.

The following plasmids were described previously: mCherry C1-Gal3,[26,62] pCR3.1-YFP-ITCH, pCR3.1-YFP-WWP1, pCR3.1-YFP-WWP2, peGFP-C1-NEDD4 and peGFP-C1-NEDD4L.[57]

pmCherry C1-ITCH was generated by amplifying human ITCH using following oligos containing KpnI (5'-TATGGTACCATGTCTGA CAGTGGATCA-3') or BamHI (5'- TATGGATCCTTACTCTTGTCCAAATCC-3') and subcloning into pmCherry C1 vector (Clontech). pCR3.1-YFP-ITCH-CA mutant (C871A) was generated by site directed mutagenesis using 5'-AGAAGTCATACCGCTTT TAATCGCCTGG-3' and 5'- GGGTAGCCAATTTTCTTTCC-3' primers.

pcDNA3 mKeima vector was generated by subcloning mKeima from pCHAC-mt-mKeima plasmid (Addgene; #72342). pcDNA3 TMEM192-mKeima was generated by amplifying human TMEM192 from HeLa cDNA using oligos containing HindIII (5'-TATAAGCT TATGGCGGCGGGGGGCAG-3') or BamHI (5'-TATGGATCCCGTTCTACTTGGCTGACAGC-3') sites and cloned into pcDNA3 mKeima vector.

Optineurin was cloned into pmCherry C2 vector by amplifying human Optineurin from HeLa cDNA using oligos containing EcoRI (5'- TATGAATTCATGTCCCATCAACCTCTCA-3') and KpnI (5'- TATGGTACCTTAAATGATGCAATCCATCA-3') sites.

SPG20 SC-helices (Helix 1, aa 418-460; Helix 2, aa 470-521; Helix 3, aa 533-580; Helix 4, aa 580-627) with a cysteine added at the N-terminus and a hexahistidine tag added at the C-terminus, were purchased as gBlocks (IDT) and cloned into pET28-MBP-TEV by Gibson cloning. TEV site in the vector was replaced with PreScission site.

Plasmid DNA was transfected using Lipofectamine 2000 (Thermo Fisher Scientific) according to manufacturer's instructions 24 hours prior to experiments.

siRNA knockdown

For human ITCH knockdown, the following siRNAs were used (purchased from Microsynth):

siITCH #1: 5'- GGAGCAACAUCUGGAUUAAUA -3' (targeting ORF; [54])

siITCH #2: 5'- GGUGACAAAGAGCCAACAGAG -3' (targeting ORF; [55])

To deplete human SPG20, the following siRNAs were used (purchased from Microsynth):

siSPG20 #1: 5'- GGCAAGGAUUGGAAUGUGCAGCUAA -3' (targeting ORF; [56])

siSPG20 #2: 5'- GGGAATCACTTATACCAAAGCCTTA -3' (targeting 3' UTR)
siSPG20 #3: 5'- GAAGGAAGAAGCAAAGAACTA -3'
siSPG20 #4: 5'- GTTGTAGCAGCAAGTAGTGTT -3'
siSPG20 #5: 5'- GTGGATTCTGCGGTCAATGTT -3'

For IST1 knockdown, the following siRNA from[32] was used (purchased from Microsynth): 5'-CCAGUCAGAAGUGGCUGAGUUGAAA-3'.

ON-TARGET plus human PI4K2A siRNA (predesigned, #1 J-006770-06-0002, #2 J-006770-07-0002) were purchased from Dharmacon.

The siRNAs (final concentration 10 nM) were transfected into HeLa cells using Lipofectamine RNAi Max according to manufacturer's instructions (Thermo Fisher Scientific) 48 or 72 hours prior to analysis. Depletion efficiency was verified by Western blot.

Cell lysis and co-immunoprecipitation

HeLa cells were rinsed twice with ice-cold PBS and lysed in lysis buffer (150 mM KCl, 50 mM Tris pH 7.4, 5 mM $MgCl_2$, 5% Glycerol, 1% Triton X-100, 2 mM β-mercaptoethanol) supplemented with protease (complete EDTA-free protease inhibitor cocktail, Roche). The soluble fractions were obtained after centrifugation at 17000 g for 5 min and directly used for SDS PAGE and western blotting or for subsequent co-immunoprecipitation experiments. For co-immunoprecipitation, cell lysates were incubated with GFP nanobody-coupled Sepharose beads for 2 h with constant rotation at 4 °C. Beads were washed 3x with ice-cold lysis buffer containing inhibitors. Proteins were eluted with Laemmli buffer, boiled at 95 °C for 5 min and analyzed by Western blotting. To detect ubiquitylation, cells were denatured in TSD buffer (50 mM Tris-HCL, pH 7.5, 1% SDS, and 5 mM DTT) and then diluted with TNN buffer (20 mM Tris-HCl, pH 7.5, 200 mM NaCl, 0.5% NP-40, and protease inhibitor cocktail).[63] The cleared lysates were incubated with GFP-coupled Sepharose beads to pull down GFP-IST1 or with primary antibody against ITCH followed by incubation with Protein G Agarose slurry (Millipore) to pull down ITCH as described above. Beads were washed 3x with ice-cold TNN buffer containing 0.1% SDS and further processed as described below for Western blotting.

Antibodies

The following primary antibodies were used in this study: anti-Spartin (SPG20) (mouse; Santa Cruz Biotechnology, sc-271888; IF 1:500; WB 1:1000), anti-SPG20 (rabbit; Thermo Fisher Scientific; PA5-65224; IF 1:500), anti-ITCH (mouse; BD Biosciences; #611198; IF 1:500; WB 1:1000), anti-IST1 (rabbit; Proteintech; 51002-1-AP; IF 1:500; WB 1:5000), anti-Gal3 (rat; Santa Cruz Biotechnology, sc-23938; IF 1:500), anti-IST1 (mouse; Proteintech; 66989-1-Ig; IF 1:500), anti-LAMP1 (rabbit; Cell Signaling Technology, #9091; IF 1:500), anti-K63-linkage specific polyubiquitin (rabbit; Cell Signaling Technology; #5621 S; IF 1:500), anti-LC3 (rabbit; MBL, PM036; IF 1:500; WB 1:2000), anti-p62 (rabbit; Sigma, P0067; IF 1:500), anti-TAX1BP1 (rabbit; Sigma, HPA024432; IF 1:500), anti-Ubiquitin (clone P4D1, mouse; Cell Signaling Technology, #3926; WB 1:1000), anti-Tubulin (mouse; Sigma, # T-5168; WB 1:5000), anti-p97 (mouse; Santa Cruz Biotechnology, sc-57492; WB 1:2000), anti-PI4K2A (rabbit; Proteintech, 15318-1-AP; WB 1:1000), anti-PLIN3 (rabbit; Proteintech, 10694-1-AP; IF 1:500) and anti-GFP (mouse; Roche, 11814460001; WB 1:10000). The secondary antibodies used in this study were as follows: horseradish peroxidase (HRP)-conjugated goat anti-rabbit IgG and goat-anti mouse IgG (1:10000, Biorad); Alexa Fluor-conjugated goat anti-rabbit, goat anti-mouse (1:500, Invitrogen) and goat anti-rat (1:500, Thermo Fisher Scientific).

Western blotting

Samples were resolved by SDS PAGE and transferred to nitrocellulose membrane (Amersham, GE Healthcare). The membranes were blocked in 3% BSA in PBST (PBS containing 0.05% Tween 20) for 1 h at room temperature (RT). Primary antibodies diluted in 3% BSA in PBST or 5% milk in PBST and incubated overnight at 4 °C or 2 h at RT. The membranes were washed 3x in PBST and incubated with secondary antibodies (diluted 1:10000 in 5% milk in PBST) for 1 h at RT. Signals were visualized with SuperSignal West Pico Chemiluminescent substrate (Pierce) or ECL Prime Western Blotting Detection Reagent (Amersham).

Immunofluorescence staining and confocal microscopy

Cells were cultured on coverslips (coverslips were coated with collagen in experiments with SH-SY5Y cells), fixed in 4% paraformaldehyde, permeabilized with 0.1% Triton X-100 in PBS for 10 min at RT and blocked with 3% bovine serum albumin in PBS with 0.1% Triton X-100 and 0.1% saponin for 1 h at RT. Primary and secondary antibodies were diluted in blocking solution and incubated on cells for 1 h at RT. Indirect immunofluorescence staining was followed by mounting in ProLong Gold (Thermo Fisher Scientific). Confocal laser scanning microscopy was performed on a TCS SP5 AOBS (Leica Microsystems) system equipped with standard PMT detectors as well as sensitive HyD detectors, a 63x/1.4 NA oil immersion objective. Lasers used were HeNe 633 nm, DPSS 561 nm, Ar 488 nm and Diode 405 nm. Acquisition and hardware were controlled by LAS AF software (Leica Microsystems) and Leica TCS SP8X Falcon confocal microscope (Leica Microsystems), equipped with HyDs SMD detectors, HC PL APO 63x/1.4 Oil CS2 objective and the Leica Application Suite X (LAS-X) software version 3.5.7. For imaging PI4K2A KO cells, Zeiss LSM800 Confocal microscope with a 63x oil-immersion objective was used and images were processed with Zen blue (v. 2.5) (Zeiss).

Live cell microscopy and photodamage

Live cell imaging was performed at 37 °C in imaging medium (P04-03591, PAN-Biotech) supplemented with 10% FCS and L-Glutamine (11500626, Fisher Scientific). For lysotracker fluorescence intensity experiment, cells were incubated with LysoTracker Deep Red (Thermo Fisher) for 1 hour and washed twice with PBS before addition of imaging medium. Prior to treatment with LLOMe, multiple regions were defined per sample for automated imaging using an Eclipse Ti-E (Nikon) inverted microscope equipped with an Andor AOTF Laser Combiner, a CSU-X1 Yokogawa spinning disk unit and an iXon3 897 single photon detection EMCCD camera (Andor Technology). CSU 640 nm laser and CFI Apo TIRF 60x/1.49 oil immersion objective (Nikon) were used for image acquisition. Every region in each sample was imaged once before addition of LLOMe and then every 5 minutes after LLOMe treatment to track loss of lysotracker fluorescence intensity from lysosomes.

Spinning disk microscopy with laser induced lysosomal damage was performed on the Eclipse Ti-E (Nikon) inverted microscope as described above. Laser lines used for excitation of EGFP and RFP were 488 nm and 561 nm, respectively. Images were acquired using a CFI APO TIRF 100x/1.49NA oil immersion objectives (Nikon). To induce LMP with light, cells were treated with 125 nM AlPcS2a (P40632, Frontier Scientific) as described before.[23] LMP was induced with a 640 nm laser with 100% power through defined regions in HeLa cells for 4 x 1000 μs pixel dwelling time using Andor Revolution FRAP and Photo Activation illumination system (FRAPPA). Image acquisition was controlled by Andor IQ3 Software (Andor Technology) as described before.[23]

Structured Illumination Microscopy (SIM)

HeLa GFP-SPG20 cells were cultured as described above and were either loaded with LysoTracker Deep Red (LysoTr) for 10 min before imaging or transfected with plasmid encoding mCherry-Optn one day prior to imaging. The cells were imaged and then treated with 1 mM LLOMe for 12 min, washed twice with PBS and further imaged either in imaging medium to track recruitment of mCherry-Optn and GFP-SPG20 or in imaging medium containing LysoTracker Deep Red to track recovery of lysotracker and recruitment of GFP-SPG20.

For timelapse recording in live cells using 2D-SIM, imaging was performed on a commercial Nikon N-SIM S microscope system equipped with ORCA-Fusion BT sCMOS camera (Hamamatsu Photonics K.K.) using NIS Elements software (Nikon). Images were acquired using a CFI SR HP Apochromat TIRF 100xAC (NA 1.49) oil immersion objective. ZIVA light engine (Lumencor) equipped with six solid-state laser lines was used as excitation light source. Laser lines used for excitation of Lysotracker Deep Red, mCherry and GFP were 637 nm, 545 nm and 476 nm, respectively. Single-band bandpass emission filters FF01-525/50 for GFP, FF01-609/54 for mCherry and FF01-692/40 for Lysotracker Deep Red (Semrock) were used. Multipoint timelapse images were acquired in three individual z-planes per position with z-spacing distance of 1 μm. Live cells were imaged once before LLOMe treatment, every 3 min during LLOMe treatment for 12 min and every 10 min after washout. 2D-SIM raw data were reconstructed using the Slice Reconstruction in NIS-Elements with default settings.

Lysophagy assay using TMEM192-mKeima cell line

HeLa TMEM192-mKeima cells were plated in 8-well Ibidi μ-slide and transfected with indicated siRNAs. After 48 hours of knockdown, live cells were imaged before and after 1 hour of treatment with 1 mM LLOMe using Leica TCS SP8X Falcon confocal microscope (specifications above) at 37 °C in imaging medium. Cells were washed twice with PBS after LLOMe treatment, maintained in imaging medium for recovery and imaged again after 6 h of chase.

Protein expression, purification, and labelling

Individual helices of SPG20 SC domain (Helix 1, aa 418-460; Helix 2, aa 470-521; Helix 3, aa 533-580; Helix 4, aa 580-627) were expressed as MBP-Cys-SPG20^{helix}-His fusion protein in *Escherichia coli* BL21 (DE3). Cells were grown in Terrific Broth to an OD_{600} of 0.8, before protein expression was induced by addition of 0.5 mM isopropyl β-D-thiogalactopyranoside (IPTG) for 16 h at 18 °C. Cells were harvested by centrifugation at 4000 g for 10 min and resuspended in lysis buffer (50 mM HEPES pH 7.4, 150 mM KCl, 25 mM imidazole, 0.5 mM tris(2-carboxyethyl)phosphine (TCEP)). Phenylmethylsulfonyl fluoride (PMSF, 1 mM) was added, cells were lysed by sonication and lysate was cleared by ultracentrifugation at 46000 g for 45 min at 4 °C. Supernatant was loaded on a 5 ml HisTrap FF column (GE Healthcare) equilibrated in lysis buffer. Column was washed with 40 column volumes of lysis buffer and eluted with 2 column volumes of lysis buffer containing 300 mM imidazole. Eluted protein was loaded on a 5 ml MBPTrap HP column (GE Healthcare) equilibrated in protein buffer (50 mM HEPES pH 7.4, 150 mM KCl, 0.5 mM TCEP). Column was washed with 8 column volumes of protein buffer and eluted with protein buffer supplemented with 10 mM maltose. Peak fractions were pooled and concentrated to 4 mg/ml for fluorescent labelling. MBP-Cys-SPG20^{Helix1}-His was incubated with 10:1 molar excess of Alexa Fluor 488 C_5 maleimide for 16 h at 4 °C for conjugation to the cysteine introduced N-terminally of SPG20^{Helix1}. Reaction was quenched by addition of dithiothreitol (DTT, 2.5 mM) before excess dye was removed by gel filtration on a Superdex 200 16/600 column (GE Healthcare) equilibrated with 50 mM HEPES pH 7.4, 150 mM KCl. Peak fractions were pooled and concentrated to 2 mg/ml. Aliquots were snap-frozen in liquid nitrogen and stored at -80 °C.

His-SPG20 and His-SPG20 8xV were cloned from human cDNA into pFL vector for expression in High Five cells (Thermo Fisher) using the baculovirus system. Four days after viral transduction, cells were harvested by centrifugation at 2000 g for 10 min and resuspended in lysis buffer. Phenylmethylsulfonyl fluoride (PMSF, 1 mM) was added, cells were lysed by sonication and lysate was cleared by ultracentrifugation at 46000 g for 45 min at 4 °C. Supernatant was loaded on a 5 ml HisTrap FF column (GE Healthcare)

equilibrated in lysis buffer. Column was washed with 40 column volumes of lysis buffer and eluted with 2 column volumes of lysis buffer containing 300 mM imidazole. Eluted protein was further purified by gel filtration on a Superdex 200 16/600 column (GE Healthcare) equilibrated with 50 mM HEPES pH 7.4, 150 mM KCl. Peak fractions were pooled and concentrated to 1 mg/ml for fluorescent labelling. His-SPG20 or His-SPG20 8xV was incubated with 10:1 molar excess of Alexa Fluor 488 C_5 maleimide for 16 h at 4 °C for conjugation cysteines. Reaction was quenched by addition of dithiothreitol (DTT, 2.5 mM) before excess dye was removed by buffer exchange to 50 mM HEPES pH 7.4, 150 mM KCl using ZebaSpin columns (Thermo Fisher). Aliquots were snap-frozen in liquid nitrogen and stored at -80 °C.

Formation of GUVs

GUVs were prepared using polyvinyl alcohol (PVA)-assisted swelling.[64] Briefly, 5% (w/w) PVA solution (weight-average molecular weight of 146000 to 186000; Sigma-Aldrich) was prepared by dissolving PVA in water at 90°C. 20 μl of the 5% PVA solution was spread on a glass slide and dried at 50°C for 30 min. Phospholipids were purchased from Avanti Polar Lipids and dissolved in chloroform to 1.3 mM concentration. 10 μl of phospholipid mixture (Table S3) at final concentration of 1 mg/ml containing AlPcS2a photosensitizer (1.3 mM in methanol) was spread on top of the PVA layer and left under vacuum for 2 hours to desiccate. 500 μl of swelling solution (280 mM sucrose and 10 mM HEPES pH 7.2) was added on this glass slide and incubated for 1 h at room temperature to induce GUV formation. Vesicles were collected by pipetting and used on the same day for microscopy and in vitro SPG20 binding assay.

GUV microscopy and in vitro SPG20 binding assay

GUVs were imaged on the Eclipse Ti-E (Nikon) inverted microscope as described in section 'Live cell microscopy and photodamage'. Oxidation of GUV membranes was induced using Andor Revolution FRAP and Photo Activation illumination system (FRAPPA) and 640 nm laser with 100% power through defined regions (45 x 90 pixels) and 1 x 100 μs pixel dwelling time for repetitive illumination every second during a period of 60 seconds. To check SPG20 binding to phospholipid bilayer, GUVs and SPG20 (1.3 μM) were mixed together and incubated for 15 minutes at room temperature before microscopy.

Image analysis and post-processing

Automated image analysis was performed on original imaging data using custom-written scripts in Cell Profiler 2.1.1. Images were manually thresholded to identify specific cellular compartments. Only cells whose whole cellular area fit within the imaging field were considered for the analysis which was limited to the cellular compartment. Identification of individual puncta of marker proteins was achieved using custom-adjusted thresholding parameters chosen to detect prominent LLOMe-induced puncta or LAMP1 lysosomal marker. Majority of the graphs represent double positive LAMP1 and LLOMe-induced puncta per cell normalized to the total number of LAMP1 puncta in a specific cell. In the case of Gal3 clearance assay, the total number of double-positive Gal3 and LAMP1 puncta per cell was quantified and cells that had more than 5 double-positive Gal3 and LAMP1 vesicles were counted and normalized to the total number of cells. Cells with more than 5 double-positive Gal3 and LAMP1 vesicles after 16 h chase following LLOMe treatment were considered as defective in lysophagy. For lysotracker fluorescence intensity measurements, individual puncta were identified and then masked as a region whose fluorescence intensity was quantified in whole.

For analysis of LysoTracker recovery following LLOMe treatment and washout, automated image analysis of timelapse recordings acquired at 2D-SIM was performed with CellProfiler (version 4.2.5)[58] Cells were detected with the Run Omnipose plugin for CellProfiler using the cyto2 model.[65] To enhance vesicular structures of both, SPG20 and Lystracker, difference of Gaussians (DoG) was applied to the respective channels. Vesicles were detected and related to the respective parent cells. Double-positive vesicles were detected using the MaskObjects module with a minimum overlap of 0.2.

For Optineurin recruitment to GFP-SPG20 positive vesicles following LLOMe treatment and washout, absolute number of GFP-SPG20 vesicles and co-localising mCherry-Optineurin vesicles were counted manually by three individuals in ImageJ and number of vesicles per cell were plotted.

Automated image analysis of mKeima ratiometric imaging was performed with CellProfiler (version 4.2.5). Briefly, cells were detected with the Run Omnipose plugin as described above. Vesicular structures were detected using the bact fluor cp model in Run Omnipose and related to their respective parent cells. The mean intensities of each channel and 561 nm/458 nm intensity ratio were measured in merged vesicular structures per cell. Minimum limits in mean red intensity, cell area and compactness of shape were used to exclude weakly expressing and dead cells from the analysis.

For in vitro SPG20 protein binding assay, original images were manually analyzed using Fiji. Background intensity was subtracted and a defined line (7 μm) was drawn through a part of each GUV membrane that was illuminated and the intensity profile of photosensitizer AlPcS2a and Alexa 488-labelled SPG20 helix 1 was plotted before and after photodamage.

Images were processed using Fiji software (https://imagej.net/Fiji), Adobe Photoshop and Illustrator.

DiGly proteomics

Cells were cultured in lysine- and arginine-free DMEM supplemented with 10% dialyzed FBS, 2 mM L-glutamine, 1 mM sodium pyruvate, penicillin/streptomycin, light (K0) lysine (38 μg/mL) and light (R0) arginine (66 μg/ml). Heavy medium was the same except the light lysine was replaced with K8-lysine (L-Lysine, 2HCl U-13C U-15N, Cambridge Isotope Laboratories Inc). Four biological

replicates of light labeled parental HeLa (ITCH WT) and heavy labeled HeLa ITCH KO cells were treated for 1 h with 1 mM LLOMe (Sigma). Cells were processed essentially as described in Fiskin et al.[66] Briefly, cells were washed twice with ice-cold PBS and scraped in 5 ml denaturing lysis buffer (8 M urea, 50 mM Tris pH 8, 50 mM NaCl, 1× PIC (protease inhibitor cocktail, EDTA-free; Roche), 50 μM DUB inhibitor PR-619 Millipore)). Samples were incubated on ice for 10 min and then sonicated with 3 × 20 s pulses. After removal of non-solubilized material (15,000 xg, 10 min, 15 °C), differentially labeled lysates were mixed at equal ratios based on total protein determined by BCA (Pierce-Thermo; typically, 10 mg of total protein). After reduction with 5 mM DTT and alkylation with 10 mM chloroacetamide, lysates were digested with 5 ng/μl Lys-C (Wako) for 1 h at RT. Subsequent digestion of peptides with trypsin (Promega) was performed as described in Villén and Gygi[67]. Desalted and lyophilized peptides were resuspended in 1.5 ml IAP buffer (50 mM MOPS (pH 7.4), 10 mM Na_2HPO_4, 50 mM NaCl) and centrifuged to remove any insoluble material (2,500 xg,5 min, 4 °C). The supernatant was incubated with anti-diGly antibody (32 μg/IP) conjugated to protein A agarose beads (Cell Signaling) for 1 h at 4 °C. Unbound peptides were removed through 3× washing with IAP buffer and once with PBS. Bound material was eluted 4× with 50 μl 0.15% TFA and peptides were desalted using custom-made C18 stage-tips (C18 material–Supelco Analytical).[68] Each sample was immunoprecipitated sequentially two times and each IP was analyzed separately by mass spectrometry.

Using an Easy-nLC1200 liquid chromatography (Thermo Fisher Scientific), peptides were loaded onto custom filled C18 reversed-phase columns and separated using a 60 min gradient of 8–80% acetonitrile containing 0.1% formic acid. Peptides were analyzed on a Q Exactive HF mass spectrometer (Thermo Fisher Scientific) using data-dependent acquisition selecting the top 5 most intense peaks from each full MS scan acquired in the Orbitrap for subsequent MS/MS while excluding peptides with unassigned charge states or charge states below +3 from fragmentation (see RAW files for specific settings). Raw data files from quadruplicate samples were processed with MaxQuant (1.6.0.1) as described previously[59,60] using a human (UP000005640) UNIPROT database and the following parameter settings: Multiplicity set to 2 with light Lys0 and heavy Lys8 labeling, first search peptide mass tolerance 20 ppm, main search peptide mass tolerance 4.5 ppm, MS/MS tolerance 20 ppm, tryptic digestion allowing up to two missed cleavages, cysteine carbamidomethylation (57.021464) as fixed modification, methionine oxidation (15.994946), N-terminal protein acetylation (42.010565) and diGG (114.042927; excluded from the C terminus) as variable modifications, revert decoy mode and peptide, protein and site FDR $\leq$ 0.01. The resulting file for diGly modified peptides was processed using Perseus (version 1.6.14.0). Briefly, common contaminants and reverse identifications were excluded resulting in 2706 unique diGly sites. Furthermore, data was filtered to keep only quantified sites present in at least three replicates reducing the sample size to 1812 unique diGly peptides. Missing values were not imputed. Statistical analysis was performed with a One-Sample t-test (p-value<0.05) with multiple comparison correction (Benjamini-Hochberg correction FDR<0.05). diGly sites were considered regulated when reaching a $\log_2$ fold change $\geq$1 or $\leq$-1 and passing the significance threshold q<0.05.

QUANTIFICATION AND STATISTICAL ANALYSIS

All quantitative data are presented as the mean ± s.e.m. or ± s.d. of biologically independent samples, unless stated otherwise. Graphs and statistical analysis were prepared using Excel (Microsoft Corporation) and GraphPad Prism 9.0 (GraphPad Software). One- or two-way ANOVA was used to determine statistical significance. Student t-tests were used to determine statistical significance where ANOVA analysis was not applicable due to the experimental setup. A p-value of <0.05 was considered statistically significant.